

NOAA Technical Memorandum ERL GLERL-36

SIMULATION OF ICE-COVER GROWTH AND DECAY
IN ONE DIMENSION ON THE UPPER ST. LAWRENCE RIVER

Gordon M. Greene

Great Lakes Environmental Research Laboratory
Ann Arbor, Michigan
June 1981



UNITED STATES
DEPARTMENT OF COMMERCE
Malcolm Baldrige,
Secretary

NATIONAL OCEANIC AND
ATMOSPHERIC ADMINISTRATION

Environmental Research
Laboratories
Joseph O. Fletcher,
Acting Director

NOTICE

The NOAA Environmental Research Laboratories do not approve, recommend, or endorse any proprietary product or proprietary material mentioned in this publication. No reference shall be made to the NOAA Environmental Research Laboratories, or to this publication furnished by the NOAA Environmental Research Laboratories, in any advertising or sales promotion which would indicate or imply that the NOAA Environmental Research Laboratories approve, recommend, or endorse any proprietary product or proprietary material mentioned herein, or which has as its purpose an intent to cause directly or indirectly the advertised product to be used or purchased because of this NOAA Environmental Research Laboratories publication.

CONTENTS

	Page
Abstract	
1. INTRODUCTION	1
2. THEORETICAL CONSIDERATIONS OF ICE-COVER GROWTH AND DECAY	5
2.1 Heat Conduction in the Ice and Snow Cover	6
2.2 Energy Balance at the Ice/Water Boundary	8
2.3 Energy Balance at the Snow/Air Boundary	9
2.4 Ice Growth	14
2.5 Ice Decay	15
3. SIMULATION MODELS OF ICE GROWTH AND DECAY	17
3.1 Surface Energy Balance Model	18
3.2 Analytical Models of Growth and Decay	28
3.3 Comparison of Models	29
4. APPLICATION OF THE SIMULATION MODELS	30
4.1 Current Ice Conditions	32
4.2 Model Testing Site and Time Period	36
4.3 Weather and Ice Conditions, Winter 1975-76	41
4.4 Simulation Results	44
5. DISCUSSION	53
6. CONCLUSIONS	56
7. ACKNOWLEDGMENTS	57
8. REFERENCES	58
9. APPENDIX A. SYMBOLS	62
10. APPENDIX B. SURFACE ENERGY BALANCE MODEL	66
11. APPENDIX C. ANALYTIC ICE GROWTH MODEL	75
12. APPENDIX D. ANALYTIC ICE DECAY MODEL	77
13. APPENDIX E. METEOROLOGICAL INPUT DATA, OGDENSBURG, N.Y.	79

FIGURES

1. Vertical section through river ice showing energy fluxes.
2. Vertical section through river ice showing model computational nodes and dimensions.
3. Energy balance model structure.
4. Structure of subroutines within energy balance model.
5. St. Lawrence River from Montreal, Que., to Lake Ontario.
6. Lake St. Lawrence outflow, 1975-76.
7. St. Lawrence River water levels, 1975-76.
8. Observed ice growth in the upper St. Lawrence River, 1975-76.
9. St. Lawrence River from **Leishman** Point to Wilson Hill Island. 40
10. Winter severity at Kingston, Ont., 1970-79. 42
11. Daily air and water temperatures, upper St. Lawrence River, 1975-76. 43
12. Ice growth simulated by analytic models. 46
13. Ice decay simulated by analytic model. 48
14. Ice growth and decay simulated by energy balance model with 2-cm node spacing. 49
15. Surface temperature simulated by energy balance model with 2-cm node spacing. 50
16. Ice growth and decay simulated by energy balance model with 4-cm node spacing. 54

TABLES

	Page
1. Physical constants used in the simulation models.	20
2. Comparison of model requirements and products.	30
3. Meteorological sensors at Ogdensburg station.	37
4. Observed ice thickness (cm), upper St. Lawrence River, winter 1975-76.	38
5. Breakup dates, Wilson Hill Island, 1972-79.	45
6. Sensitivity analysis for energy balance model, maximum ice thickness.	52
7. Sensitivity analysis for energy balance model, date of breakup.	55



SIMULATION OF ICE-COVER GROWTH AND DECAY IN ONE DIMENSION
ON THE UPPER ST. LAWRENCE RIVER*

Gordon M. Greene

A series of models are presented for simulating the growth and decay of channel ice in one dimension on the upper St. Lawrence River. By assuming simplified boundary conditions and a linear temperature gradient in the ice layer, I have been able to treat the theory of ice growth analytically, producing the first group of models. A less abstract approach was taken in the construction of a deterministic surface energy balance model. This model simulates the relevant energy fluxes at the upper and lower boundaries of the snow/ice cover on the river. In addition, the model simulates the diffusion of heat through the ice layer, permitting the absorption of shortwave radiation within the ice and the use of a model time step of less than 24 h.

A general description of ice growth and decay is given for the reach of the river between the Moses-Saunders Power Dam at Cornwall, Ont., and Lake Ontario. Simulation sites in both slow moving and faster reaches of the river are discussed. Over the winter of 1975-76, the analytic model produced results well correlated with observed ice thickness during growth. During decay, the results simulated in a slow moving reach are much closer to observed thickness than are those simulated in a faster reach.

The energy balance model simulates a maximum ice thickness that is 75 percent of the observed thickness. In addition, the simulated maximum thickness **occurs** 2 weeks later than the observed maximum. These shortcomings appear to be caused by model node geometry and by the absence of turbulent heat transfer between the ice and the river. The model does simulate ice-cover breakup within the period when breakup was observed to occur. Sensitivity analysis of the model suggests that the simulated results are **most** sensitive to variations in air temperature, water temperature, and net radiation. Thermodynamic processes appear to be sufficient to produce breakup without the additional simulation of mechanical forces.

1. INTRODUCTION

The decay and destruction of a river ice cover is a complex process involving mechanical and thermal energy transfer between the ice, the water, and the atmosphere. One measure of the level of understanding of this interaction is the degree to which the various processes can be simulated or

*GLERL Contribution No. 259.

modeled. The purpose of this paper is to describe the structure and application of models designed to simulate the growth and decay of a highly abstract, one-dimensional ice cover formed on the St. Lawrence River. In particular, the study site is found on the international section of the river, running for 169 km between Lake Ontario and Cornwall, Ont.

The goal of simulation modeling is the accurate representation of complex events, such as the decay of an ice cover. Once one has constructed a model that adequately mimics past events, the model can be used to extend the simulated processes into the future. The only restriction as to how far into the future the model can accurately predict is the degree to which realistic input variables can be forecast.

There are a number of reasons why the ability to predict ice decay rates is important for the St. Lawrence River. Despite its role as a major transportation corridor, the river is unusable for up to 4 months of the year. An accurate projection of the river's opening date is important because of the economic benefits of advance planning. For instance, ships from European ports must time their departure so as to arrive at the St. Lawrence River as soon as possible after the river is open for passage.

The second major economic function of the river is to generate electricity. Although maximum flow is desirable for power production at the Moses-Saunders Power Dam (located just upstream of Cornwall), the river flow must be controlled during the decay period to help ensure an orderly breakup. A better prediction of breakup would lead to more accurate planning of power generation.

Two basic approaches are possible when attempting to predict events. The first approach is statistical, extrapolating from past records to predict future events. For example, if accumulated degree-days are found to be well correlated with the date of breakup, observers would only need to forecast one variable, air temperature, to assign a probability to the projected date of breakup. Such an approach, however, masks understanding of the various processes at work in a decaying ice cover. In addition, the statistical approach assumes stationarity for meteorological and hydrological conditions over time. Recent work by Assel (1980) concerning trends in winter severity over the Great Lakes points out the fallacy of this assumption.

Theoretical models, on the other hand, integrate understanding of all relevant processes such that the models simulate both the intermediate steps and the eventual outcomes. The theoretical models described in this work couple the components of surface energy flux, the turbulent heat flux from the river water, and the processes of heat transfer within the snow and ice layers. These models then simulate changes in ice-cover thickness and temperatures at fixed time intervals.

The advantage of such a model over the statistical approach is that one can test the model to discern those processes that have the most influence on the timing and magnitude of ice growth and decay. Prediction then becomes a matter of forecasting only the most influential variables, not because they correlate best with events, but because they have the most power to explain future events.

Before continuing, it is necessary to understand the **various ways** the word "breakup" is used in this study. In general, "breakup" has been used to refer to both the set of processes causing the destruction of an ice cover and to the time period over which those processes are occurring (Marshall, 1978). To reduce ambiguity, this report uses "breakup" to refer to the processes of melting, crystal structure deterioration, and the mechanical destruction caused by the action of winds and currents. The phrase "breakup period" refers to the time interval over which these processes are active. In general, the phrase spans the time from maximum ice thickness to the complete absence of ice in the river.

Qualifications are necessary, however, to keep the notion of breakup period meaningful. In the climate of the St. Lawrence region, it is possible to get mid-winter thaws and storms that break up the ice cover temporarily. Only the last of these periods in the spring is considered to be the breakup period.

The first date on which the river channel is completely ice-free is termed the "breakup date," ending the breakup period. It must be noted, however, that ice in the bays and shoreline areas can be found more than 3 weeks after the channel ice is gone from the river channel. Because of the transportation emphasis of this study, the breakup date will only be defined by the absence of channel ice. In addition, the model breakup date will be defined as the date on which the model ice thickness is reduced to 0 cm.

There are many characteristics of river ice that obscure the processes under study and hence the ability to model ice decay. As described by Ashton (1978):

Much of the understanding of river ice that we presently have is based on the assumption that river ice occurs in a steady or quasi-steady state. This is far from the case. Instead, it would be most accurate to summarize river ice processes as a series of steady states that exist between short periods of intense activity and change. These short periods, while most significant in establishing the next steady state, are also the most difficult to observe, analyze, predict, or otherwise understand.

As a result of this uncertainty, breakup dates for rivers tend to be more variable from year to year than do those for lake or sea ice under the same climatic conditions (Bilello, 1980). River ice breakup is commonly described as the result of two sets of processes. The first set brings about changes in the ice cover itself, either by melting or by reducing the strength of the ice. The second set are the products of increased flow on the ice cover, i.e., the process of the ice being swept downstream. In order to adequately predict the beginning of mechanical breakup, therefore, one would need to monitor four determinant influences (Shulyakovskii, 1966): the state of the ice cover before melt begins, the input of heat and radiation to the ice cover, stream flow forces, and the resistance of the shores to ice drift.

Unlike most rivers, however, the upper St. Lawrence has a number of characteristics that help to maintain quasi-steady-state conditions on the river. The source of water for the river is a large, deep reservoir, which cools very slowly in autumn and warms slowly in spring. The temperatures of the water flowing into the St. Lawrence, therefore, are much more stable than one would find in a river with extensive headwaters and tributaries. Additionally, the relative proportion of flow contributed by tributary streams and rivers is small, ranging from 1 to 4 percent of the flow measured at Cornwall.

The most significant influence on breakup characteristics, however, is the St. Lawrence Seaway Power Project at **Massena**, N.Y. The operation of the power dam at this site controls the outflow of the upper St. Lawrence and can be used to a certain extent to attenuate the forces of breakup.

While a large body of literature exists concerning Arctic and sub-Arctic rivers, little work has been done to analyze the ice cover of large rivers in the temperate zone. **Bilello (1980)**, for example, has surveyed the growth and decay patterns of 16 Canadian and Alaskan rivers. Only sites north of 50°N latitude were chosen, however, to avoid rivers with mid-winter thaw and refreezing cycles. Michel (1973) and Williams (1970) have also described patterns of decay in Canadian rivers, but avoided regulated rivers, such as the St. Lawrence. An example of Russian work is that by **Antonov et al. (1973)**, classifying Siberian rivers into four types based on breakup characteristics.

Despite geographical differences, however, descriptions of the processes at work in decaying ice are applicable to the St. Lawrence. In this area of study, the literature is extensive. **Ashton's** work on heat transfer to river ice (1973, 1978) is primarily theoretical, concentrating on the fluid dynamics beneath the ice sheet. Others, such as Weeks and **Dingman (1973)**, Michel (1971), and **Pivovarov (1973)** have concentrated on the thermal processes that shape the ice cover. Mechanical properties of river ice relevant to breakup analysis are described by **Korenkov (1970)** and **Bulatov (1973)**.

For ice on the St. Lawrence River itself, detailed year-to-year information on ice conditions and river operations is contained in the Navigation Season Extension Studies published by the St. Lawrence Seaway Authority, a Canadian organization under the Marine Transportation Authority. Their published reports start with the 1972-73 winter season and extend to the present. The most comprehensive description of ice conditions and types on the St. Lawrence River is contained in Marshall (1978).

The importance of transportation on the river has stimulated a large number of studies of heat loss from the river as the water cools to the ice point. The usual approach of these studies is to compute a total heat loss coefficient that, when applied to estimated travel times and air - water temperature differences, most accurately reflects the observed temperature drop. This work was initiated by Barnes (1906) and revitalized by Kerry (1946). Since then, a number of studies have attempted to refine the methods. **Ince and Ashe (1964)** used empirical relationships between air temperature and the heat budget components to compute total heat loss for the river over time. **Dingman et al. (1967, 1968)** used a more theoretical approach to compute the

heat budget terms in order to study how increased river water temperatures could maintain ice-free stretches of the river. Witherspoon and Poulin (1970) used the same approach except that they defined a cooling coefficient to determine heat loss.

The energy balance model described in this paper extends this approach by continuing to compute the relevant heat fluxes after ice has formed. The magnitude and direction of the total flux then controls the rate of growth and decay. Similar approaches have been used by Maykut and Untersteiner (1969) for sea ice and by Anderson (1976) for a snow pack.

The model used for this study is derived from a surface energy balance simulation described by Outcalt and Carlson (1975). Their model was also applied in a modified form to simulate the thermal structure of Lake Ohrid, Yugoslavia (Outcalt and Allen, 1980).

2. THEORETICAL CONSIDERATIONS OF ICE-COVER GROWTH AND DECAY

In order to discuss the theory of ice-cover growth and decay, it is helpful to examine a diagram of the system that controls the transfer of heat from the river water through the ice and snow layers to the air. Figure 1 shows four layers extending from the river water to a height above the river surface where meteorological observations are made. In between are the ice layer and the snow layer.

Such a representation of the river ice system implies that a number of assumptions have been made about the fluxes of mass and energy. The primary assumption is that the ice cover is already in place. This report does not consider the significant issue of how ice initially forms, either from the energy balance viewpoint of forecasters (e.g., Adams, 1976) or from detailed study of frazil ice formation (e.g., Carstens, 1970; Michel, 1971).

Each layer is considered to be a **homogenous** material with uniform properties. All mass and energy fluxes are considered only in the vertical direction. Energy is assumed to be absorbed at idealized boundaries, which are flat and have no thickness. The transfer of heat from the ice to the snow is continuous.

Changes in mass are possible at either the upper or the lower surface of the system. At the snow surface, snowfall can occur, as well as the melting of snow and ice. At the lower boundary, ice growth and thaw will occur. All forcing meteorological variables, such as air and water temperatures used to compute surface energy fluxes, change in uniform, discrete time steps. The thickness and structure of the ice cover is such that snow ice never forms.

It is assumed that no frazil ice collects at the bottom of the ice layer and that the temperature at the ice/water interface, T_m , is equal to 0°C . All water temperatures are considered to be homogeneous because of turbulent mixing of the flow, except for a 5-cm boundary layer at the bottom of the ice cover. No geothermal heat flux from the river bed is considered.

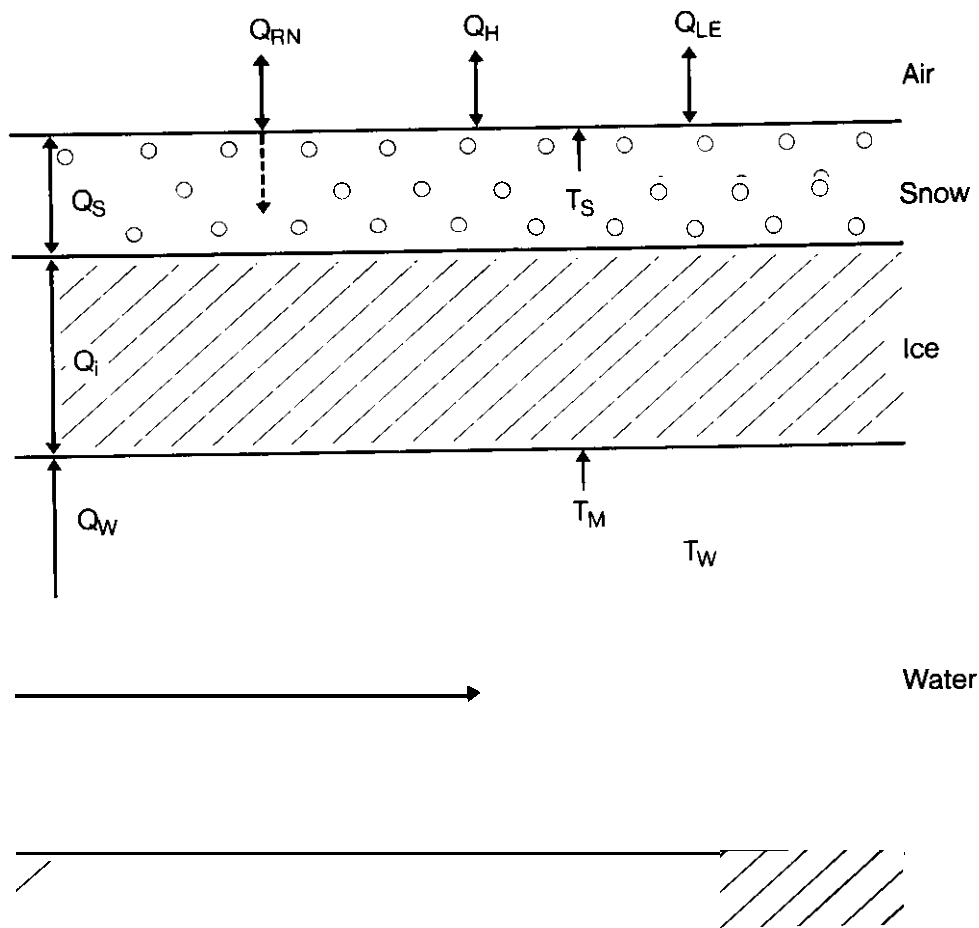


FIGURE 1.--*Vertical* section through river ice showing energy fluxes.

The discussion of applicable theory has been divided into five sections: a discussion of heat flux within the snow and ice layers, energy balance at the ice/water boundary, energy balance at the snow/air boundary, ice growth, and ice decay.

2.1 Heat Conduction in the Ice and Snow Cover

Vertical heat flow in simplified, **homogenous** materials can be summarized by two equations. The first is the common defining equation for heat flux, where

$$Q = -K \frac{dT}{dZ} . \quad (1)$$

K is thermal conductivity ($W m^{-1} \text{ } ^\circ C^{-1}$), T is temperature ($^\circ C$), and Z is depth (m).

Secondly, one can describe the change in heat flux with depth as

$$\frac{dQ}{dZ} = -C \frac{dT}{dt} , \quad (2)$$

where C is thermal heat capacity ($J m^{-3} \text{ } ^\circ C^{-1}$) and t is time (s). By substitution, and with the assumption that thermal conductivity is not a function of depth, the general heat conduction equation in one dimension can be written

$$\frac{dT}{dt} = \frac{K}{C} \frac{d^2 T}{dZ^2} . \quad (3)$$

Both numerical and analytical approaches can be used to solve equations (1) and (2). For ease of solution, common analytical methods assume periodic or step functions for the upper thermal boundary conditions and frequently employ linear thermal gradients with no heat flux divergence. In this work, only discrete step boundary conditions are considered. While the following section describes the finite difference numerical method used in the model, this section considers the application of analytical solutions to the river ice system.

Under equilibrium conditions, when no flux divergence is taking place, the temperature gradient through the ice layer is constant. Equation (1) can be rewritten as

$$Q_i = \frac{K_i (T_m - T_s)}{Z_i} , \quad (4)$$

where T_s and T_m are the temperatures ($^\circ C$) at the top and bottom of the ice layer, respectively.

As will be discussed, however, there are a number of reasons why it is desirable to allow flux divergence within the ice. In nature, shortwave radiation absorbed within the ice cover functions as an internal heat source. In this case, the governing heat conduction equation becomes

$$\frac{dT}{dt} = \frac{K}{C} \frac{d^2T}{dz^2} + \frac{k}{C} Q_{sw} (1-A)e^{-kz} , \quad (5)$$

where k is the bulk extinction coefficient (m^{-1}), A is surface albedo, and Q_{sw} is the shortwave radiation incident on the surface ($W m^{-2}$). The right-hand term thus produces heat flux divergence because the value decreases as a function of depth.

2.2 Energy Balance at the Ice/Water Boundary

In figure 1 it can be seen that there are two energy fluxes at the ice/water boundary: the flux of heat from the water to the ice, Q_w ($W m^{-2}$), and the flux of heat within the ice cover, Q_i ($W m^{-2}$). These two fluxes are related by the change in ice thickness

$$Q_i - Q_w = \rho_i \lambda \frac{dz_i}{dt} , \quad (6)$$

where ρ_i is ice density ($kg m^{-3}$), and λ is the latent heat of fusion ($J kg^{-1}$). Unlike turbulent transfer in the air, the transfer of heat beneath the ice cover has received little attention. As a first approximation, one can reason that heat transfer is primarily a function of the temperature difference between the ice and the water

$$Q_w = h_i (T_w - T_m) , \quad (7)$$

where h_i is an empirical turbulent transfer coefficient ($W m^{-2} ^\circ C^{-1}$) and T_w is the river water temperature.

Ashton (1979) gives an empirical derivation of h_i based on a description of turbulent transfer in closed conduits. The basic form of the equation relates the rate of transfer to the Reynolds and Prandtl numbers

$$\frac{h_i R}{K_w} = B Re^{0.8} Pr^{0.4} \quad (8)$$

where B is an experimentally derived coefficient and R is the hydraulic radius (m). By computing expected values of the Reynolds and Prandtl numbers at $0^\circ C$ and letting the hydraulic radius, R , equal half the water depth, Z_w (m), Ashton (1979) describes h_i as a function of water speed and depth

$$h_i = B_i \frac{U_w^{0.8}}{Z_w^{0.2}} . \quad (9)$$

One limitation to this transfer coefficient is that the conduit walls are assumed to be smooth. Especially in spring when water temperatures rise, ripples form on the underside of the ice, transverse to the direction of flow. Under these conditions, B_i may need to be increased by as much as 50 percent in order for equation (8) to correctly describe the rate of melt.

2.3 Energy Balance at the Snow/Air Boundary

Energy balance at the snow/air interface must be considered under two conditions, with and without phase change. When no phase change is occurring, T_s is assumed to be less than 0°C . During spring melt, the upper snow layer or the upper surface of the ice is melting and T_s is fixed at 0°C . Considering the first case, one can assume that the flux of heat to the surface from below must equal the flux of heat leaving the snow surface under equilibrium conditions

$$Q_s = -Q_t . \quad (10)$$

Q_t (W m^{-2}) is the sum of the relevant fluxes as defined by

$$Q_t = Q_{rn1} + Q_h + Q_{le} , \quad (11)$$

where Q_{rn1} is the net longwave radiation flux (shortwave radiation is absorbed internally), Q_h is sensible heat flux to the air, and Q_{le} is latent heat flux.

In discussing all fluxes, this paper follows the convention that any flux away from the surface in either an upward or downward direction is negative. The relevant equations for computing the net radiation flux and the turbulent transfer of sensible and latent heat are outlined below.

2.3.1 Net Radiation

Net radiation is the steady-state balance of incoming to outgoing longwave radiation.

$$Q_{rn1} = Q_{r1} - \epsilon \sigma (T_s)^4 , \quad (12)$$

where Q_{r1} is the atmospheric longwave radiation (W m^{-2}), ϵ is surface emissivity, and σ is the Stefan-Boltzmann constant.

The description of atmospheric radiation from surface measurements has remained a problem in **microclimatology**. While it is generally accepted that clear sky values can be described as a function of air temperature and water vapor near the ground's surface, these relationships are not valid under cloudy conditions since the cloud base acts as a full radiator. The generalized method of allowing for cloud **cover** (Sellers, 1965) **is** based on

$$Q_{r1} = Q_{r1} (1 + an^2). \quad (13)$$

clear sky

In this relationship, "n" is the fraction of sky covered with clouds and "a" is a **constant** that allows for the decrease in cloud base temperature with increasing cloud height.

But because cloud base height **or** even cloud type is not commonly available for many sites, another method of adjusting for cloud presence must be used. The method used here is based on the Anderson-Baker formulation (1967), which was developed from and tested at a number of sites **across** the United States.

$$Q_{r1} = [\sigma(T_a)^4 - [(110.6 + 5.41(e_a^{0.5} - e_s^{0.5})) - 0.485 E] \left(\frac{Q_{sw}}{Q_{swc}}\right)^2] \quad (14)$$

The formulation of the above relationship is begun with the clear sky **longwave** radiation as a function of screen level air temperature (T_a), water vapor pressure in the air (e_a), and ground level water vapor pressure (e_s). A station-specific adjustment term, E, a function of the long term relationship between air temperature at the surface and at one level in the upper atmosphere, is then applied. Finally, the ratio of observed shortwave radiation, Q_{sw} , to the potential clear sky shortwave radiation, Q_{swc} , is applied as a factor, decreasing the clear sky **longwave** radiation value.

At the one site in northeastern United States where observed atmospheric **longwave** radiation data are available (Lebanon, N.H.), Anderson and Baker (1967) found a correlation coefficient of 0.92 between observed and estimated daily **longwave** radiation **over** a 6-month winter period. Give" the fact that shortwave radiation data are also needed for the surface energy balance model and in the absence of specific cloud data, this Anderson-Baker method is used here as a first approximation. Greene (1981) describes the equations used in computing the solar geometry and atmospheric attenuation that define clear sky shortwave radiation, Q_{swc} .

2.3.2 Turbulent Transfer

A discussion of turbulent heat transfer to the air in the **most** rigorous form is outside the scope of this report. Excellent reviews are provided by

Anderson (1976), Dyer (1974), and Male and Granger (1978). Instead, this section concentrates on the determination of turbulent fluxes when only one level of meteorological observation is available.

The basic equations for the vertical transfer of momentum (τ), sensible heat (Q_h), and latent heat (Q_{1e}) are expressed as

$$\tau = \rho_a D_m \frac{dU}{dz} \quad (15)$$

$$Q_h = -\rho_a c_p D_h \frac{dT}{dz} \quad (16)$$

$$Q_{1e} = -\rho_a \lambda D_w \frac{dq}{dz} \quad (17)$$

The D values are eddy diffusivities that can be considered analogous to molecular diffusivities.

If these equations are integrated between Z_a (m); the height at which wind speed, air temperature, and water vapor observations are made; and Z_0 (m), the aerodynamic roughness length, the transfer equations become

$$\tau = \rho_a C_m U^2 \quad (18)$$

$$Q_h = -\rho_a c_p C_h U (T_a - T_s) \quad (19)$$

$$Q_{1e} = -\rho_a \lambda C_w U (q_a - q_s) \quad (20)$$

The C values are dimensionless numbers called bulk transfer coefficients. Note that, although Z_0 is some distance above the surface where wind speed becomes zero, the temperature and moisture conditions at Z_0 are assumed to be the same as at the surface.

Under conditions of neutral stability over uniform surfaces, profiles can be described by a logarithmic decay curve

$$U = \frac{U^*}{\nu K} \ln \frac{Z_a}{Z_0} \quad (21)$$

By substitution it can be shown that

$$C_M = \frac{(vK)^2}{Z_a^2 \ln\left(\frac{Z_a}{Z_0}\right)} . \quad (22)$$

Equation (21) suggests that the value of a transfer coefficient is a function of the shape of the wind profile, which in turn is a function of atmospheric stability. Quinn (1979) has described an extension of the bulk transfer coefficient t'' different stability conditions by reevaluating equation (21) along the lines first described by Businger et al. (1971).

$$u = \frac{U^*}{vK} \left(1'' \left(\frac{Z_a}{Z_0} \right) - \psi_1 \right) \quad (23)$$

Using a similar line of reasoning,

$$T_a - T_s = T^* \left(\ln \left(\frac{Z_a}{Z_0} \right) - \psi_2 \right) . \quad (24)$$

where T^* is a scaling temperature defined by

$$T^* = -\left(\frac{1.}{vK U^*} \right) \left(\frac{Q_h}{\rho_a c_p} \right) . \quad (25)$$

The ψ terms are derived as functions of a stability ratio, Z/L , where L is the **Monin-Obukhov** length. Four stability classes are considered:

unstable	$Z/L < 0,$
neutral	$Z/L = 0,$
stable	$0 < Z/L < 1,$ and
strongly stable	$Z/L > 1.$

By substituting the right-hand side of equation (19) into equation (25), substituting for T^* in equation (24), and solving for C_h , a stability corrected bulk transfer coefficient can be found

$$C_h = \frac{vKU^*}{U(\ln(\frac{z_a}{z_o}) - \psi_2)} \quad (26)$$

By assuming that the transport mechanisms for sensible and latent heat are similar, equation (26) is also valid for C_w .

Most of the experimental studies that have been used for validating the ψ functions have been performed **over** bare ground **or** short vegetation. Few studies have examined their **use over snow or ice**, where one would frequently expect strongly stable conditions.

Anderson (1976) describes a surface energy balance model that does incorporate stability corrected turbulent flux relationships into a snow melt model. While the model closely mimics observed **snow** melt, the lack of observed turbulent fluxes prevents real validation.

Working in a prairie environment, Male and Granger (1978) have compared various methods of determining turbulent transfer **over snow** with measured fluxes. They found that the bulk transfer coefficient method can cause **errors** when computing flux values **over** melting **snow** surfaces. One explanation of the **error** is that radiant heating of the air close to the **snow** pack creates a temperature maximum a few centimeters above the surface rather than at the surface. The effect of such a shift would reverse the direction of the **computed** turbulent flux. Such an effect does not seem critical in the St. Lawrence River area because **most** of the melt of the upper layer takes place when the air temperature is greater than the assumed surface melt temperature of 0°C.

A **more** serious conclusion from Male and Granger, however, is that the bulk transfer equation may overestimate evaporation. They present **some** evidence suggesting that the transfer mechanisms for latent and sensible heat **over** melting snow are not equivalent as was assumed.

An approach simpler than the analytical determination of each of the turbulent fluxes has often been used in energy balance simulations (e.g., Ince and Ashe, 1964; Witherspoon and Poulin, 1970). Basically, Q_t , the heat leaving the surface, is considered to be a function of the temperature difference between the air and the water surface in a relation analogous to equation (7)

$$Q_t = h_a (T_s - T_a) \quad (27)$$

Williams (1963) has best described the advantages and limitations of such an approach. He points out that the equation allows for heat transfer by convection and by net **longwave** radiation. However, neither shortwave radiation nor evaporation are direct functions of the air - surface temperature difference. It can be correctly applied only in those cases where the shortwave radiation net gain and evaporative loss are equal in magnitude.

2.4 Ice Growth

Analytically, it is difficult to describe ice growth under all but the most simplified conditions. A common set of boundary conditions is that air temperature is equal to the surface temperature ($Q_h = 0 \text{ W m}^{-2}$) and does not vary with time. Turbulent transfer between the river water and ice is neglected and the snow layer is not present. substituting T_a for T_s and substituting equation (4) into equation (6),

$$\rho_i \lambda \frac{dZ_i}{dt} = \frac{K_i (T_m - T_a)}{Z_i} . \quad (28)$$

Integration over time leads to the classic Stefan solution.

$$Z_i = \left(\frac{2K_i}{\rho_i \lambda} \right)^{\frac{1}{2}} \left[\int_0^t (T_m - T_a) dt \right]^{\frac{1}{2}} \quad (29)$$

Note that this equation has the form

$$Z_i = F(S)^{1/2} , \quad (30)$$

where S is the accumulated freezing degree-days.

The effect of a snow layer is to decrease the rate of growth. Using the same boundary conditions and assuming that heat flux through the ice is equal to the flux through the snow layer,

$$\rho_i \lambda \frac{dZ_i}{dt} = \frac{(T_m - T_a)}{\frac{Z_i}{K_i} + \frac{Z_s}{K_s}} . \quad (31)$$

After integration

$$Z_i^{t+1} = \left[\left(Z_i^t + \frac{K_i}{K_s} Z_s \right)^2 + \frac{2K_i}{\rho_i \lambda} S \right]^{1/2} - \left(Z_i^t + \frac{K_i}{K_s} Z_s \right) , \quad (32)$$

where "t" and "t + 1" refer to the time interval. By using equation (27), one can allow convective transfer to take place from the snow/ice layer. The case without a snow layer is

$$\rho_i \lambda \frac{dz_i}{dt} = \frac{(T_m - T_a)}{\frac{z_i}{K_i} + \frac{1}{h_a}} \quad (33)$$

With a snow layer, equation (31) becomes

$$\rho_i \lambda \frac{dz_i}{dt} = \frac{(T_m - T_a)}{\frac{z_i}{K_i} + \frac{z_s}{s} + \frac{1}{a}} \quad (34)$$

2.5 Ice Decay

As discussed in the introductory section, use of the word "breakup" implies large-scale destructive processes. However, Michel (1971) points out that two different sets of processes are occurring at different rates. The first set includes the slow processes of weakening and melting of the ice cover. For these processes the time scale is in days and weeks, with events occurring primarily in the vertical dimension through the snow ice cover. The second set of processes results in the cracking of the ice cover into floes and their movement downstream. In this case, critical events occur over time scales in minutes and days and must be considered in all three dimensions over large reaches of the river at any one time.

As will be discussed in the chapter describing model applications, the second set of processes are not particularly relevant to the St. Lawrence River above Cornwall owing to the volume and regulation characteristics of the flow. In this reach, breakup is largely a function of ice deterioration, with thermal effects playing a large role (Marshall, 1978, 1979); therefore, discussion of ice decay will focus on the processes that weaken ice in one dimension. This includes snow melt, melting at the top and bottom of the ice layer, absorption of shortwave radiation within the ice, and precipitation effects.

The theory of snow melt is complex owing to the coupled flows of water, water vapor, and energy and the corresponding change in the physical properties of the snow pack (Yen, 1969; Dybig, 1977). With increasing radiation absorption and air temperature in spring, the snow surface warms to 0°C, at which point phase change can take place. Equation (10) becomes

$$Q_t + Q_s = \rho_s \lambda \frac{dz_s}{dt} \quad (35)$$

Melt water produced at the surface infiltrates the **snow** pack, warming the layer to the freezing point as the melt water refreezes. Once the **snow** pack is isothermal, additional ablation lowers the **snow** surface. Equation (35) also applies to the upper ice surface **once** this **snow** layer is melted.

Spring rains also have a considerable effect on upper surface melt, even though the thermal effects in one dimension of a given rainfall are minimal. For example, 2.5 cm of rain with an average temperature of 10°C contains enough heat to melt 0.9 cm of **snow** initially at -5°C. The same rain falling on the ice sheet could melt 0.3 cm of ice initially at -5°C. On the other hand, rainfall causes considerable changes in the snow and ice-cover texture, which in turn speed up other processes of decay. Among these are increased **snow** density, cracking due to the additional weight on the ice cover, and a decrease in **albedo** due to the ponding of water. In addition, the concentration of water flow on an irregular surface creates channels and sink holes in the ice surface (Marshall, 1978).

Melting also occurs at the bottom of the ice layer. In using equation (6) so far, the effects of Q_w , turbulent transfer between the water and the ice, have been ignored. While Q_w is usually much smaller than Q_i during the ice growth period (Ashton, 1973), its effect is significant **once** water temperature **starts** to rise. Ashton (1973) has developed an integrated form of equation (6), with the boundary condition that maximum ice thickness, Z_{max} , occurs at time 0. Solving for the time interval,

$$\Delta t = \frac{-\rho_i \lambda (Z_i - Z_{max}) - k_i \rho_i \lambda (T_m - T_s)}{Q''} \cdot \frac{1 - \frac{Q_w Z_i}{k_i (T_m - T_s)}}{1 - \frac{Q_w Z_{max}}{K_i (T_m - T_s)}} \quad (36)$$

By specifying the time interval of interest, it is possible to use numerical methods to find an approximate solution for Z that represents the ice thickness after a given period of bottom melt caused by turbulent transfer. As noted above, ripples are commonly formed on the underside of the ice, perpendicular to the flow, which considerably alters the magnitude of turbulent transfer (Ashton, 1978).

As shown in equation (5), all shortwave radiation not reflected at the surface is assumed to penetrate the ice cover. While a number of studies have affirmed that the attenuation can be adequately described by Beer's law (Maykut and Untersteiner, 1971; Maguire, 1975), the vertical heterogeneity in river ice would preclude the use of a bulk extinction coefficient assumed

to be constant with depth (Shishokin, 1969). Beer's law is used in the surface energy balance model as a method of roughly describing the decrease in radiation absorption with depth, but it should not be construed as physical reality. In this work, the law is expressed as

$$Q_z = Q_{sw} (1. - A) e^{-kz} . \quad (37)$$

Observation of ice candling in spring clearly shows that radiation is absorbed along crystal boundaries, producing weakly bonded columns of ice perpendicular to the ice cover, with water along these crystal boundaries (Michel and Ramseier, 1970). After sufficient weakening, a thick layer of ice can be shattered by a sharp blow, such as by a floating ice floe.

Bulatov (1973) has attempted to quantify this decrease in strength. He suggests that the strength of ice at a given cross section is proportional to the relative area of solid phase

$$\frac{SIG}{SIGO} = 1. - X , \quad (38)$$

where X is the relative area occupied by a liquid. SIG is the melting ice cover breaking stress, and SIGO is the breaking stress at 0°C without the effect of the absorbed radiation. Bulatov also describes this ratio as a function of absorbed radiation

$$1. - x = (1. - (\frac{ST}{STO})^{1/2})^2 , \quad (39)$$

where ST is the amount of heat absorbed at a given depth and STO is the heat equivalent of the ice if melted. He has found a range of 6.7×10^7 to $23.0 \times 10^7 \text{ J m}^{-3}$ for STO, but uses $1.84 \times 10^8 \text{ J m}^{-3}$ as an average representative of the mean composition of reservoir and river ice.

3. SIMULATION MODELS OF ICE GROWTH AND DECAY

Two simulation models were constructed to simulate the growth and decay of the ice cover on the St. Lawrence River. The first is a detailed surface energy balance model that first computes energy transfer at the ice/air boundary and then adjusts the thermal profile within the ice layer. The second model combines the degree-day growth represented by equation (34) with the ice melt caused by rising water temperature, as shown in equation (36). The application of both models to a site on the St. Lawrence is discussed in the next section. This section discusses the construction and operation of each of the models.

3.1 Surface Energy Balance Model

This model is based on the energy balance relationship described by equation (11). The principle feature of such a model is that it couples processes occurring both in the air above the ice and in the water below the ice with energy transfer within the snow/ice layers. Unlike the simplified analytic solutions discussed in the theory section, this model permits finite difference solutions to the transfer of heat within the snow/ice layer. Ice thickness as such is never the variable to be evaluated. Rather, a simple check of the simulated temperature at each computation node determines whether that node exists in the ice phase or not. Figure 2 shows the one-dimensional structure assumed for the model operation. Computation node LICE is considered to be fixed, while LSNOW, LBOT, and LFIX change in accordance with snowfall, ice growth, and melting, respectively. The height, Z_s , of the meteorological observations is considered as fixed, a valid assumption as long as Z_s is small compared to Z_a . Features of this model include the fact that it allows for a wide range of atmospheric stability. In addition, it allows a non-linear temperature gradient to evolve in the ice and permits shortwave radiation to be absorbed internally rather than at the surface.

The particular temperature diffusion method used allows a large range of time intervals and computation node geometries to be used within the model. The choice of a daily time step and 2-cm computation node spacing was suggested by the maximum ice cover observed, the availability of input data, and the projected use of the model for breakup forecasts.

Input data needed for the model can be divided into three groups: initial conditions, forcing meteorological parameters, and physical constants. The model starts on a given day with a known ice and snow layer thickness. All computation nodes at or above LICE (or LSNOW, depending on the presence of snow) are assigned the first day's air temperature, and all nodes below LBOT are assigned the observed water temperature. The temperature at LBOT is 0°C , and all ice layer temperatures are interpolated between the surface temperature and 0°C .

In order for the model to operate, one must supply mean daily values of wind speed, air temperature, dew point temperature, water temperature, and total daily incident shortwave radiation. The first three variables are measured at one height, a known distance above the surface. Model operation assumes that each variable is constant over a 24-h period, with an instantaneous change to the next day's value. To justify equation (11), one must assume that an equilibrium surface temperature also exists for each day's condition and also undergoes instantaneous change to a new steady state the next day. In contrast, it is not necessary for temperature profiles in the snow/ice layer to come to equilibrium each day. The section on model sensitivity discusses the relative impact of each of these variables on model operation.

Table 1 lists the physical constants employed in the model. Some of these "constants" can show a considerable range of values in nature. Therefore, sensitivity of the model to variations in von Karman's constant, aerodynamic roughness length, and albedo are also considered.

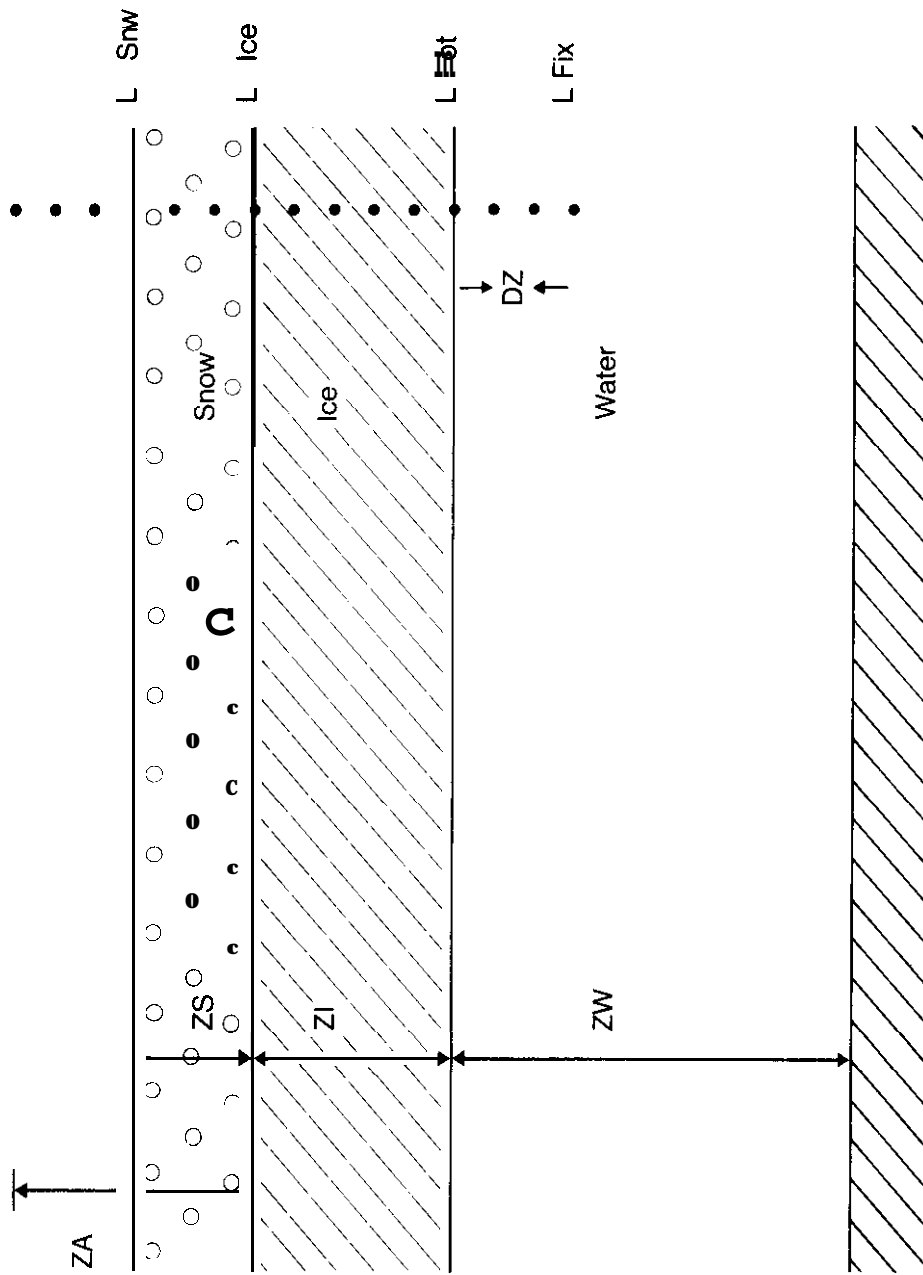


FIGURE 2.- Vertical section through river ice showing model computation nodes and dimensions

TABLE 1.--Physical *constants used in the simulation models*

Symbol	Definition	units
AT	Model time interval	8.64 x 10 s
ΔZ	Distance between model computation nodes	2 cm
E	Station adjustment to equation (13)	33. (Bolsenga, 1967)
DUST	Dust content of the atmosphere	1. particles cm ⁻¹
σ	Stefan-Boltzmann constant	5.67 x 10 ⁻⁸ W m ⁻² K ⁻⁴
vK	von Karman constant	0.41 (Dyer, 1974)
A	Snow albedo	0.85 (Bolsenga, 1977)
A _i	Ice albedo	0.55 (Bolsenga, 1977)
k	Shortwave radiation bulk extinction coefficient	2.0 m ⁻¹ (Shishokin, 1969)
Z _a	Height of meteorological observations	10 m
Z _o	Aerodynamic roughness length of snow	7.0 x 10 ⁻⁴ m (Michel, 1971)
ρ_s	Snow density	350 kg m ⁻³
K _w	Water thermal conductivity (Sellers, 1965)	5.74 x 10 ⁻¹ W m ⁻¹ °C ⁻¹
K _i	Ice thermal conductivity (Sellers, 1965)	2.18 W m ⁻¹ °C ⁻¹
K _a	Air thermal conductivity (Sellers, 1965)	2.51 x 10 ⁻² W m ⁻¹ °C ⁻¹
K _s	Snow thermal conductivity (Yen, 1969)	2.68 x 10 ⁻¹ W m ⁻¹ °C ⁻¹
α	Thermal diffusivity of snow	3.81 x 10 ⁻⁷ m ² s ⁻¹ (Yen, 1969)

Model output includes simulated surface temperature, net radiation flux, turbulent fluxes, sensible heat flux with the snow/ice layer, snow thickness, ice thickness, and the temperature at each of the model nodes in the snow and ice layers.

3.1.1 Main Program (I)

The program GGRIV simulates river ice growth and decay using the surface energy balance approach. The main program, outlined in figure 3, is comparatively simple, leaving the bulk of the computations to the subroutines shown in figure 4 and described below. Within the main program there are essentially three steps, which are repeated for each simulated day. Once the initial conditions are described, these steps are: 1) read in the forcing meteorological data, then 2) solve for the equilibrium surface temperature by a call on SEARCH, and finally, 3) adjust the temperature profile in the snow/ice layer. The rationale behind steps 2) and 3) need more discussion before individual descriptions of each subroutine. In the equations used to describe the fluxes impinging on the snow/ice surface, all variables except T_s , the surface temperature, are provided or could be derived. It is possible, however, to use numerical methods to find the one temperature value that would enable equation (11) to sum to zero.

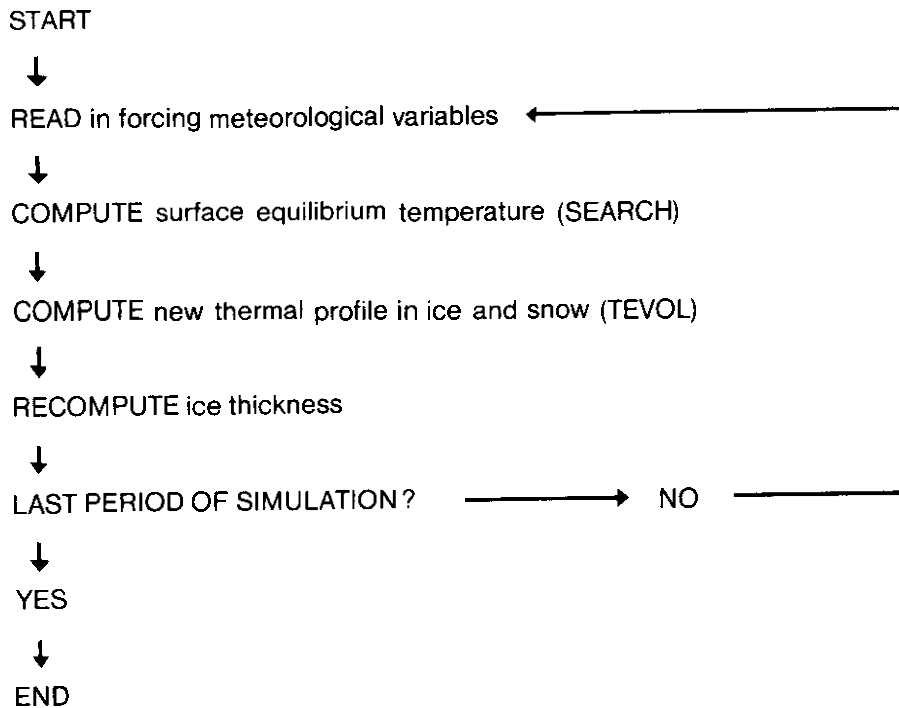


FIGURE 3. -- Energy balance model structure.

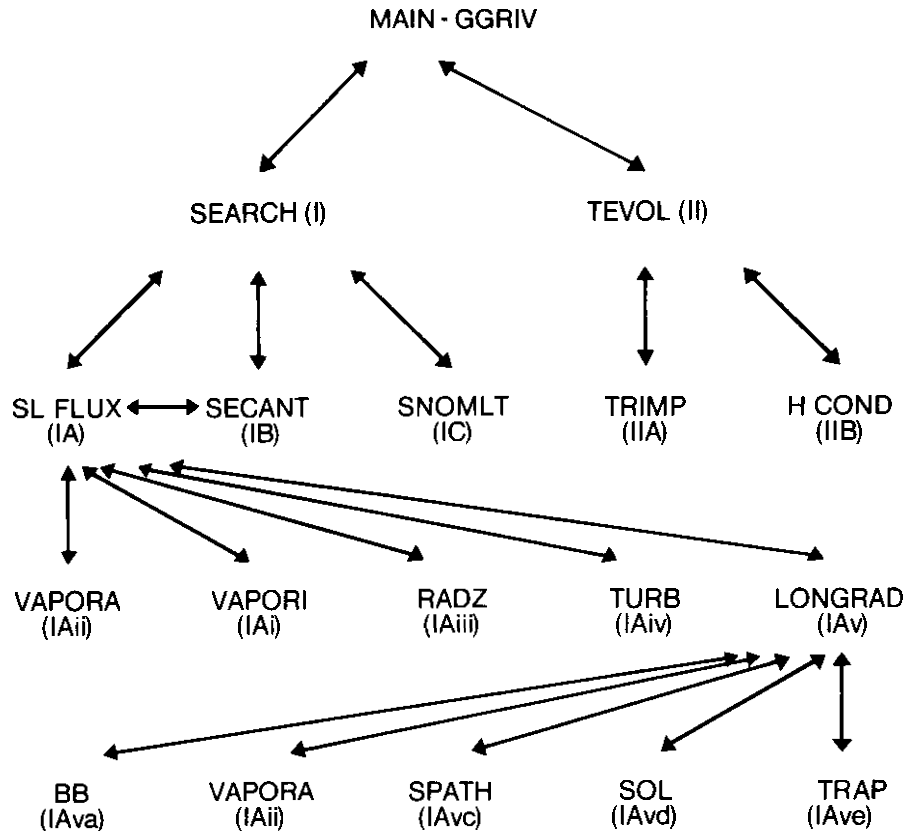


FIGURE 4.--Structure of subroutines within energy balance model.

The surface temperature is then used as an upper boundary condition necessary for the numerical solution of equation (3). With the upper boundary fixed by T_s and the lower boundary fixed by the known water temperature beneath the ice, it is possible to simulate the flow of heat through the snow and ice leading to growth or decay.

3.1.2 Subroutine SEARCH (IA)

This subroutine keeps track of changes in the snow layer depth and controls the search for the surface equilibrium temperature (T_s). First a high and then a low estimate is made of the surface temperature. With each estimate, a call is made on SLFLUX to compute the four energy balance components. Their algebraic sum, BAL, is used with subroutine SECANT to make the next estimate for surface temperature. Once BAL falls within an acceptable range of 0 W m^{-2} , the last estimate becomes the daily equilibrium surface temperature. If T_s is greater than 0°C , but a snow layer exists, T_s is set equal to 0°C . Another call is made on SLFLUX, and SNOMLT is called to determine how much ablation could take place.

3.1.3 Subroutine SECANT (IB)

This subroutine is based on a numerical method for solving a set of equations transcendental in one variable (Beckett and Hurt, 1967), temperature in this case. If $f(T)$ equals BAL, the residual sum of the four energy balance fluxes in equation (11), then a new estimate for the temperature can be found by

$$T_n = T_{n-1} - (((T_{n-1} - T_{n-2}) * f(T_{n-1})) / (f(T_{n-1}) - f(T_{n-2}))), \quad (40)$$

where n is the iteration number. This T_n is returned to SEARCH and then sent to SLFLUX.

3.1.4 Subroutine SNOMLT (IC)

When the simulated equilibrium surface temperature is greater than 0°C , melt can take place. T_s is reset to 0°C and heat exchanged by conduction, Q_s , is assumed to be 0 W m^{-2} . The heat flux now available for melting is found by restating equation (11) as

$$\text{FLUXIN} = \text{RN} + \text{H} + \text{LE}. \quad (41)$$

The heat flux needed to bring each layer, DZ, of the snow pack to 0°C is computed as

$$\text{HCOUNT} = (\text{T}(\text{LSNOW}) - \text{T}(\text{L})) * \text{DZ} * \text{SNOCAP}, \quad (42)$$

where SNOCAP is the thermal heat capacity of the snow.

HCOUNT for each layer is then compared to FLUXIN, starting at the top of the snow pack. When FLUXIN is no longer larger than HCOUNT for a layer, the loop is ended, and the remaining FLUXIN is saved as RMDR, to be added to the right side of equation (11) at the next iteration, with a new set of forcing meteorological values. If surplus flux is available for melting during a given time step (MELT = 1), the amount removed by ablation, ABLA, is computed as

$$\text{ABLA} = \text{FLUXIN} / (\text{LH} * \text{SNODEN}), \quad (43)$$

where LH is the latent heat of fusion and SNODEN is the snow density.

3.1.5 Subroutines TEVOL (II) and TRIMP (IIA) and Function HCOND (IIB)

The diffusion of heat through the snow/ice layer is based on a fully implicit solution to equation (3) described by Outcalt and Carlson (1975). In finite-difference form, the equation becomes

$$T_1^{t+1} = T_1^t + \frac{\alpha \Delta t}{(\Delta Z)^2} (T_{1+1}^t + T_{1-1}^t - 2T_1^t), \quad (44)$$

where superscript t refers to time and subscript 1 refers to computation node. If the Fourier modulus, F , is defined as

$$F = \frac{\alpha \Delta t}{(\Delta Z)^2}, \quad (45)$$

the above equation becomes

$$T_1^{t+1} = FT_{1-1}^t + (1 - 2F)T_1^t + FT_{1+1}^t. \quad (46)$$

In this explicit form, the model is unstable with an F greater than 0.5 since that makes the central term in the above equation negative. The implicit solution of Outcalt and Carlson (1975), however, reverses time and obtains a stable solution in the following form

$$T_1^t = -FT_{1-1}^{t+1} + (1 + 2F)T_1^{t+1} - FT_{1+1}^{t+1}. \quad (47)$$

Variables needed to compute the diffusion of heat are

T(L)	temperature at each node
Z(L)	distance of each node from the upper reference surface
DT	time step.

In addition, the locations of the interfaces LBOT, LZ, LSURF, and LEQ, shown in figure 2, are needed. Intermediate values supplied or computed within TEVOL are

DIF	thermal diffusivity
XA, XW, XI	volume fractions of air, water, and ice, respectively
CON	thermal conductivity
CAP	volumetric heat capacity
FU	upper Fourier modulus
FB	lower Fourier modulus
A(L), B(L), C(L), D(L)	vectors for the diffusion subroutine TRIMP
C1	empirical parameter used to define the shape of the temperature-heat capacity curve
LF	latent heat of fusion
HK(I)	volume fraction thermal conductivity.

The first step in TEVOL is to define the thermal diffusivity at each computation node. For the water and snow layers, this value is assigned. But both volumetric heat capacity and thermal conductivity are functions of the amount of water present when freezing takes place, and therefore diffusivity must be derived for the ice layer. For heat capacity

$$XW = \text{EXP}(C1 * T(L)) * (1. - XA) \quad (48)$$

$$XI = (1. - XW - XA) \quad (49)$$

$$CAP = XW + 0.48 * XI + (LF * C1 * XW) \quad (50)$$

Thermal conductivity, CON, is then computed within function HCOND as a function of the individual volume fraction thermal conductivities from equations modified by **Outcalt** (1977) from Philip and **DeVries** (1957).

$$CON = \frac{\sum_{I=1}^3 S(I) * X(I) * HK(I)}{\sum_{I=1}^3 S(I) * X(I)} \quad (51)$$

where $(X(I), I=1,3)$ represents the volume fractions of air, water, and ice. The shape factor, $S(I)$, is defined as

$$S(I) = \frac{(X(I)/HK(I))}{\sum_{I=1}^3 (X(I)/HK(I))} . \quad (52)$$

Therefore, when phase change is taking place,

$$DIF = CON/CAP. \quad (53)$$

Restating equation (45), we now have

$$F = (DIF*DT)/(ZN)^2 , \quad (54)$$

where ZN is the computation node spacing. The F values for each node are then used to fill the vectors sent to TRIMP, where the implicit method described by **Outcalt** and **Carlson** (1975) solves for $T(L)$

$$A(L) = C(L) = -F \quad (55)$$

$$B(L) = 1. + 2F \quad (56)$$

$$D(L) = T(L). \quad (57)$$

One problem that occurs with a time step as large as 1 day is that the abrupt changes in the meteorological variables from day to day can force temperatures in the ice to appear to skip the interval between 0°C and -1°C , where phase change effects are most pronounced. If this skip seems to occur, the diffusivity is not decreased by the temporary increase in heat capacity, and thus ice growth is abnormally fast. The use of $C1$ in the computation of XW as a function of temperature extends the region where water still exists to a point around -2.0°C .

3.1.6 Subroutine SLFLUX (IA)

This subroutine and its subsidiaries compute the four surface energy balance components of equation (11). In addition, when the snow layer has been melted it calls RADZ, computing the rise in temperature at each computation node caused by the absorption of shortwave radiation. Q_s is the only flux actually computed within SLFLUX. The other fluxes are computed within TURB and LONGRAD.

3.1.7 Functions VAPOR1 (IAi) and VAPORA (IAii)

These functions compute the saturation vapor pressure (in mb) for a given temperature at the snow/ice surface and in the air, respectively. The formula used is based on a polynomial expression derived by Lowe (1977). Compared to the standard Goff-Gratch formulations, Lowe's method is accurate, yet requires much less computational time.

3.1.8 Subroutine RADZ (IAiii)

This subroutine supplies the right-hand term of equation (5), computing the rise in temperature caused by shortwave radiation absorption, **TRAD**.

$$\text{TRAD} = \text{RSN} * (\text{XK} / \text{C}) * \text{EXP}(-\text{XK} * \text{ZR}) \quad (58)$$

The selection of an appropriate bulk extinction coefficient (XK) is a difficult problem for two reasons. One is the high sensitivity of **TRAD** to this term. Secondly, few studies exist that report values for XK. In this case, values were chosen from Maguire (1975), even though he only measured radiation attenuation between 400 and 700 nm in ice on the Ottawa River.

3.1.9 Subroutine TURB (IAiv)

This subroutine uses the method described by Quinn (1979) to allow for atmospheric stability effects when computing Q_h and Q_{le} . An initial guess is made for both the friction velocity, **USTAR**, and the Monin-Obukov length, **XL**. These are then used to derive the ϕ factors, which in turn compute new values for **USTAR** and **XL**. A numerical iteration is made in order to converge computed ϕ values, stopping when the change becomes less than 0.1 percent. The final **USTAR** is then used to compute the bulk transfer coefficient, C_h , as described by equation (26). Equations (19) and (20) then compute Q_h and Q_{le} , respectively.

3.1.10 Subroutine LONGRAD (IAv) and Function BB (IAvi)

This subroutine computes net longwave radiation from mean daily values of air temperature, moisture content, and the simulated surface temperature. Longwave radiation received from the sky hemisphere is computed with equation (13) from Anderson and Baker (1967). The value for E , the station adjustment factor, is taken from Bolsenga (1967). In order to adjust for the effect of cloud cover, it is also necessary to compute the ratio of received shortwave radiation, Q_{sw} , to potential shortwave radiation, Q_{swc} . Instantaneous values at hourly intervals of Q_{swc} are computed by subroutines SPATH and SOL. These in turn are integrated into potential daily total by subroutine TRAP. Function BB computes the blackbody radiation at the simulated surface temperature with the Stefan-Boltzman relationship.

3.1.11 Subroutine TRAP

This subroutine is a numerical method for integration by the **trapezoidal** rule. The code was taken directly from Beckett and Hurt (1967).

3.1.12 Subroutines SPATH and SOL

These subroutines are used to compute the potential shortwave radiation received at the ice surface. SPATH, based on Sellers (1965), computes the solar geometry at a given time. SOL first computes radiation received at a surface "outside" the atmosphere and then adjusts for atmospheric attenuation by absorption and scattering. The algorithm for attenuation is best described in **Outcalt and Carlson** (1975). Note that hemispheric shortwave radiation, HEM, includes both diffuse radiation and simulated backscattering from the ice surface.

3.2 Analytical Models of Growth and Decay

In addition to the surface energy balance model, three analytical models of ice growth and one model of ice melt were used to simulate ice processes on the St. Lawrence River. Program DEGD (listed in appendix C) contains the ice growth algorithms, and program MELT (listed in appendix D) simulates ice ablation.

Within DEGD, HTOT1 is the maximum possible ice growth as computed from the integration of equation (28). The temperature at the bottom of the ice slab, T_b , is constant at 0°C and the upper surface temperature is equivalent to the daily mean air temperature. Freezing degree-days (DD2) were only accumulated usually once actual ice growth had begun, in early January, rather than in mid-November, when mean daily air temperatures below 0°C first occurred.

Using the same assumption as equation (28) but allowing a snow layer to accumulate, the model also computes HTOT5. Since equation (32) is only valid for constant snow layer thickness, the model integrates step-wise, so that the daily difference of air temperature and 0°C, DELT, is used in place of S. H5 represents the incremental growth for that day.

As discussed above, it is also analytically possible to allow for turbulent transfer from the ice surface, so that the surface temperature is no longer set equal to the air temperature. Such an approach requires the use of a transfer coefficient. Intuitively, such a coefficient would seem to be a function of wind speed and ice thickness. As a first approximation, however, a constant value of $11.6 \text{ W m}^{-2} \text{ }^\circ\text{C}^{-1}$ was applied (Williams, 1963). This equation (34) was computed within DEGD in finite difference form. Each day's incremental growth was computed as

$$\Delta Z_i = \frac{(0. - T_a) A t}{\left(\frac{Z_i}{K_i} + \frac{1}{h_a} + \frac{Z_s}{K_s}\right) \rho_i \lambda} \quad (59)$$

so that

$$HTOT4 = Z_i + \Delta Z_i \quad (60)$$

Program MELT is based on Ashton's (1973) integration of equation (6) as described by equation (36). Note that no snow layer is present and that T_a is presumed equal to T_s . Q_w is computed from equations (9) and (7), where B_i takes on the value $1622 \text{ W m}^{-2.6} \text{ s}^{0.8} \text{ }^\circ\text{C}^{-1}$ (Ashton, 1979).

The above equation must be solved for that Z_i that brings the right-hand side of the equation equal to the time interval. While the secant algorithm already described could be used, a simpler approach was chosen. Small increments of NI, the initial ice thickness, were subtracted from NI and then substituted into equation (36). Once the right-hand side came within an acceptable range of the time interval, NI was redefined by the successful choice for thickness.

Data requirements for all four of these models are extremely simple. For the growth models, mean daily air temperature is the only required input data. Physical constants are supplied internally. The only specification of initial conditions is the day when ice growth started.

In the analytic melt model, mean daily air and water temperatures are used. One specifies a water depth and current speed beneath the ice. This speed is assumed constant over the simulation time period. In addition, the model requires the maximum ice thickness and the date of its occurrence. Table 2 compares the relative needs and products of models GGRIV, DEGD, and MELT.

3.3 Comparison of the Models

The energy balance and analytic models differ in three areas. The primary difference is that the energy balance model does not assume a linear temperature gradient through the ice. The temperature diffusion scheme used allows for the absorption of shortwave radiation in the ice cover.

A second difference is that the operation of the energy balance model is **continuous**; that is, melting begins at the time of simulated maximum ice thickness and not at the observed maximum.

Finally, the models differ in the boundary fluxes they incorporate. The energy balance model incorporates all surface fluxes but conduction only between the ice and the water beneath. The analytic growth models excluded all turbulent fluxes at both the upper and lower boundaries. The analytic melt model includes turbulent transfer at the lower boundary but none at the upper surface.

TABLE Z.--Comparison of *model* requirements and products

Models	Input data	Initial conditions	Output
GGRIV	T_{dp} , T_a , T_w , U , Q_{sw}	Thickness of initial cover, date of initial cover	Ice thickness, energy balance fluxes, snow and ice temperature
DEGD	T_a	Date to start accumulating degree-days	Ice thickness
MELT	T_a , T_w	Maximum ice thickness, date of maximum ice thickness	Ice thickness

4. APPLICATION OF THE SIMULATION MODELS

As discussed in the introduction, the energy balance and analytic models described were designed to be used on the St. Lawrence River, specifically on the international section stretching between Cornwall and Lake Ontario. Figure 5 shows the form of this section of the river, the principal towns, and significant seaway structures. The upper reaches of the river between Kingston, Ont., and Chippewa Bay are broad and filled with hundreds of islands. The river then narrows down to a 65-km stretch extending as far as Waddington, N.Y. Below this stretch, the river broadens into Lake St. Lawrence, created by the Moses-Saunders Power Dam just upstream from Cornwall.

It is important to differentiate between the St. Lawrence River and the St. Lawrence Seaway. While the river is the entire stretch of water just described, the seaway is a system of man-made locks, canals, ice booms, the Iroquois control dam, and the Moses-Saunders Power Dam that allows the river to be used for commercial transportation. This work, except for ice boom installation, was completed in 1958, considerably altering the hydrology of the river. Operation of the seaway during its first winter demonstrated the necessity of installing ice booms to further stabilize the ice cover in order to decrease the amount of frazil generated in the river. Booms were subsequently designed and used as part of the seaway operation.

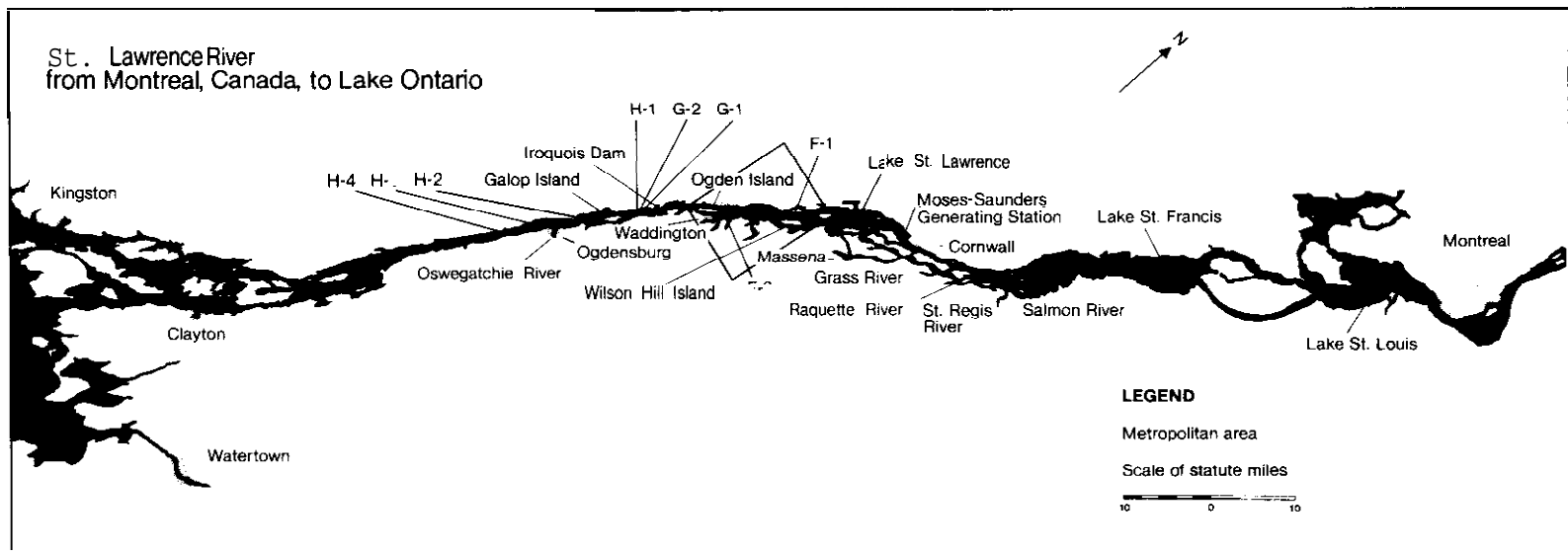


FIGURE 5.--St. Lawrence River from *Montreal, Que.*, to Lake Ontario.

Prior to the completion of the Moses-Saunders Dam, the gradient of the river was **much** steeper than its present value. Starting at Lake Ontario, the river decreased in height very slowly until a sudden 3-m drop at the downstream end of Galop Island. From there, the river dropped another 25 m on its way to Cornwall.

As a consequence of these gradient changes, the ice structure on the St. Lawrence was much different than one finds currently. In early winter a natural ice bridge would form, stretching between Prescott, Ont., on the north bank and Ogdensburg, N.Y., on the south bank. The relatively flat upper river water would freeze **over** behind this bridge. In the steep section below this area, considerable **frazil** ice "as produced because the water "as kept open by the rapids below Galop Island. This **frazil** tended to collect and jam near Cornwall, leading to spring floods (Acres American, Inc., 1978).

4.1 Current Ice Conditions

This section discusses the ice patterns currently characteristic of the upper St. Lawrence River, both along its length and in cross sections. This information is derived from field observations, examination of aerial photographs, and reports by Marshall (1978, 1979).

In general, freeze-up on the St. Lawrence proceeds from the downstream reaches up toward Lake Ontario. In an average winter, the upstream advance of the ice cover from Montreal to Lake St. Lawrence takes 3-4 weeks, yet takes only 2-10 days to cover a comparable distance from Lake St. Lawrence to Lake Ontario. In a mild winter, freeze-up is usually complete by early February, in an average winter by mid-January, and in the **most** severe cases, by late December.

Looking at the river in cross section, one can discuss a number of stages in the formation of ice. The shallow bays, occurring either naturally or at the margins of the lakes created by the seaway, are the first areas to freeze. With little or no water current, ice forms in a way analogous to lake ice. This shallow water cover is in place roughly 30 days before the channel sections are ice covered. Ice thickness at the river margins is likely to be as much as 20-30 percent greater than that found in mid-channel. The proportion of lake ice to **snow** ice in a given vertical section also changes as one moves from shore areas to mid-channel. The percentage of **snow** ice is greater close to shore because of flooding though the hinge cracks at the edge of the ice cover.

In the channel areas, ice-cover formation is different from the processes found near shore. **Frazil** and slush gradually agglomerate into ice floes **over** a period of weeks. These floes initially collect at the borders of the bay ice **or** in places where the flow is constricted. As the **areal** density increases, they congeal into a solid ice cover, with a thickness ranging from 4 to 15 cm.

Secondary ice growth in the channel then occurs beneath the primary layer over a **5-7-week** period. In addition, **snow** saturated by rain or by river

water rising through stress cracks freezes and forms snow ice. But even during the most severe winters, the deep-channel portion of the river is not completely ice covered. There are many regions where open water pools remain owing to the upwelling of bottom currents caused by river bottom topography or to flow over the dams at Iroquois, Ont., and Cornwall.

In general, ice decay in the international section of the river follows a pattern opposite to that described for ice-cover formation; that is, the uppermost reaches of the river are the first to become ice free. The breakup of the ice cover is now much more orderly than in the period before the construction of the seaway because of the lower gradient and the predominant effect of thermal processes. The beginning of ice-cover erosion is determined primarily by the rising river water temperature, which in turn depends on the rate of decay of the Lake Ontario ice cover.

Initially, ice in the channel areas is weakened both by the internal absorption of shortwave radiation (candling) and by the percolation of melt water downward along the crystal boundaries. In addition, the ice cover melts at the base as the water temperature increases and the current increases. From the air, the thinner areas appear as dark patches and streaks in the ice cover, usually concentrated near stretches of open water. As the ice weakens between pools of open water, it begins to fail due to current action.

This ice becomes a moving stream of brash ice, breaking through zones of weak ice or hanging up at the upstream edge of stronger ice. Eventually, under the influence of currents, the moving brash is formed into strands of ice that stretch over many miles. These individual chunks then melt owing to increased absorbed solar radiation or convective heat transfer with air and river water.

This general discussion of ice formation and decay on the St. Lawrence River must also take into account the effect of the seaway. The operating principle for the Moses-Saunders Dam is to maintain a stable ice cover, while minimizing hydraulic head losses. This balance is critical because operating the dam in a way that optimizes power production could create a river velocity high enough to considerably delay ice-cover formation, allowing additional frazil ice to form.

Ice booms are set in place at four locations when river temperatures at the Moses-Saunders Dam reach 39°F. These booms are set at Ogdensburg-Prescott to reinforce the formation of the natural ice bridge already described, at Chimney Point, and in the Galop Island area, still the region of highest water velocity.

As air and water temperatures decrease in autumn, the length of water generating frazil increases. This ice is caught at the power dam, the Galop boom, and the Ogdensburg boom. Once the ice pack starts to consolidate at these points, flow at the power dam is purposefully decreased to lower the river velocity, increasing the speed of ice-cover formation. These manipulations of the river outflow and subsequent changes in water level can be seen in figures 6 and 7. Figure 6 shows the outflow from Lake St. Lawrence at the Moses-Saunders Dam over the 1976 winter. There is a sharp drop in the outflow

LAKE ST. LAWRENCE OUTFLOW

34

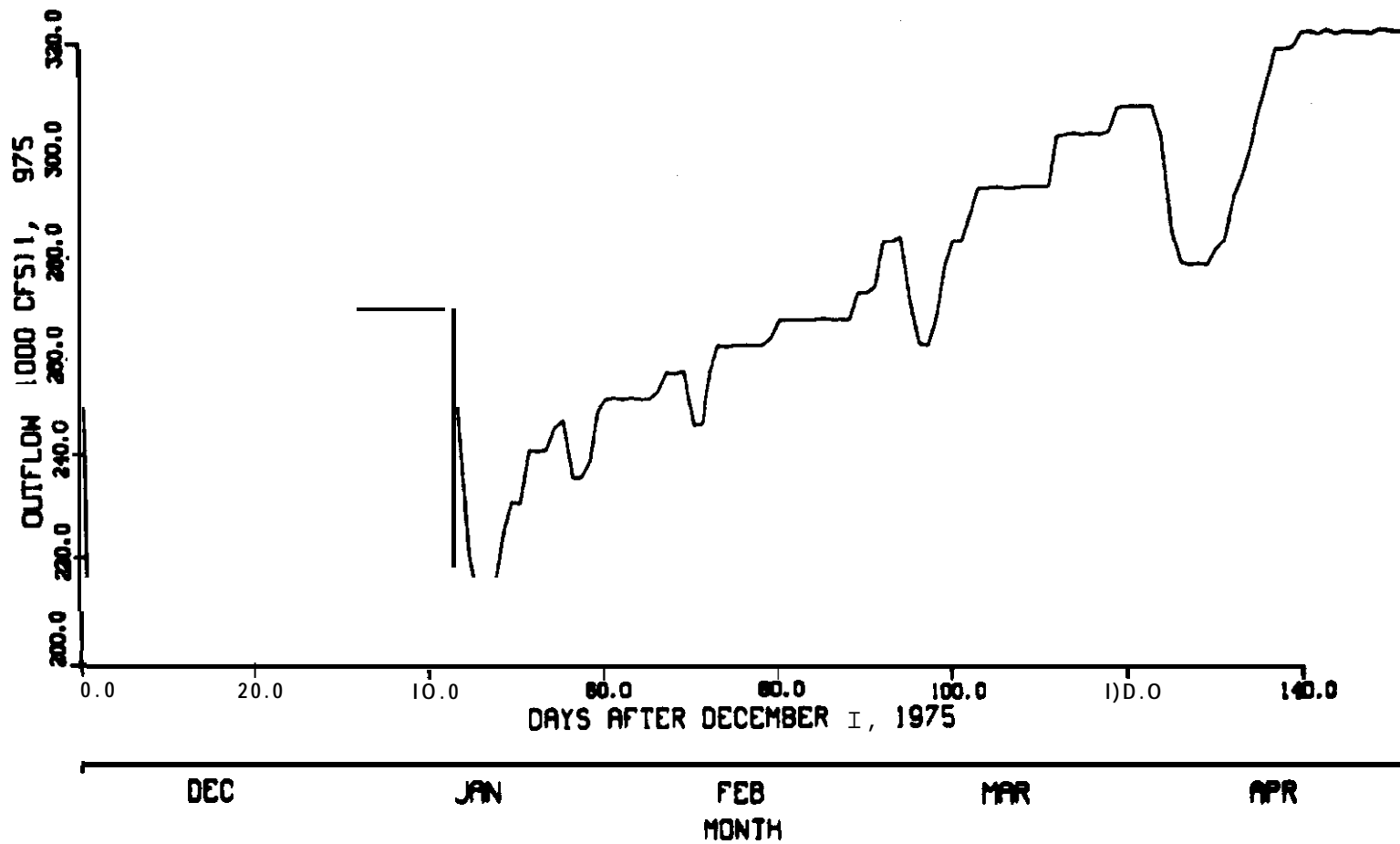


FIGURE 6.--Lake St. Lawrence outflow, 1975-76.

ST. LAWRENCE RIVER WATER LEVELS

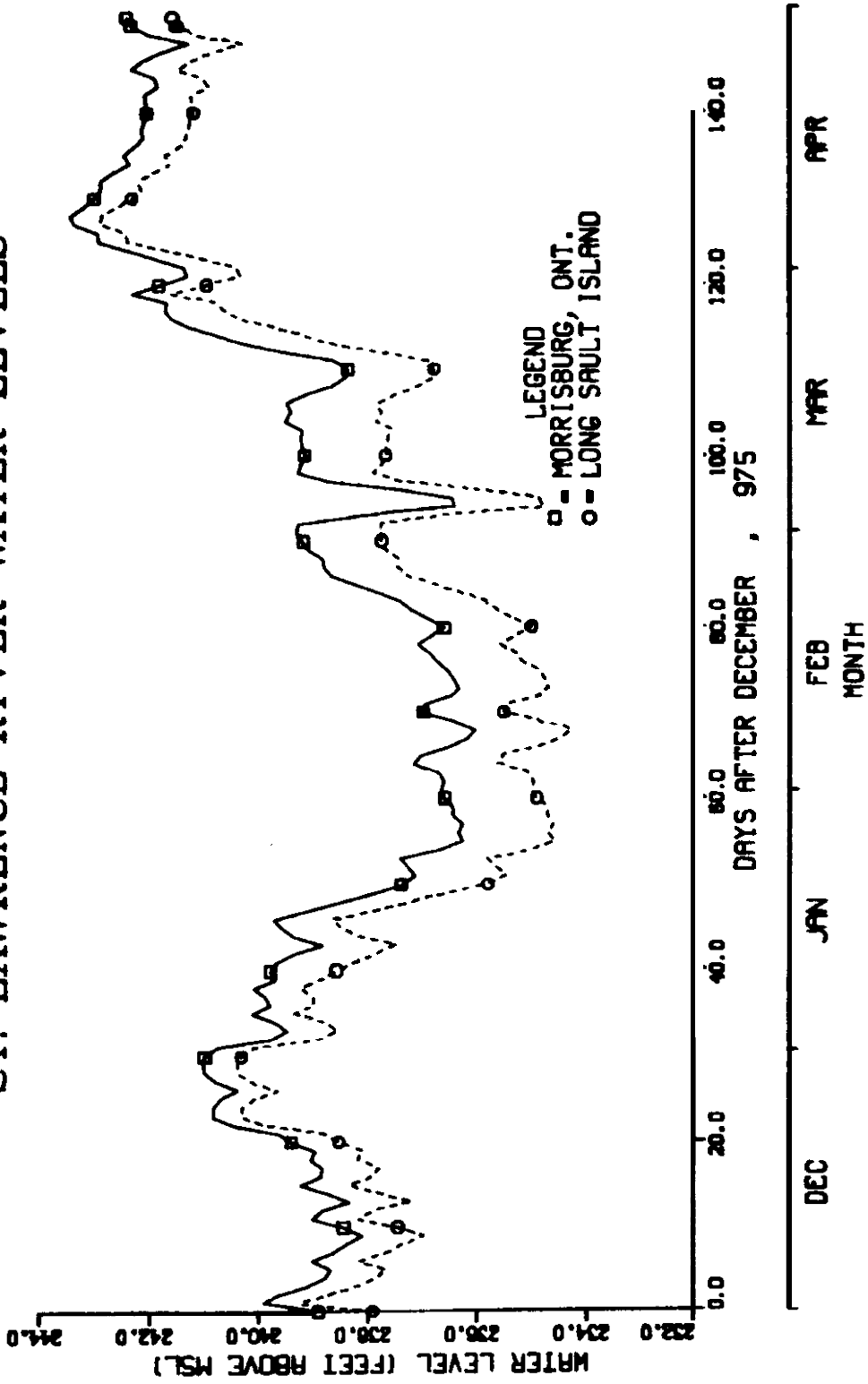


FIGURE 7.- St. Lawrence River water levels, 1975-76.

in January, consequent with the consolidation of the ice cover in Lake St. Lawrence. Figure 7 shows the river water level at Morrisburg, Ont., (30-km upstream from the dam) and at Long Sault Island (8-km upstream from the dam).

While the general water level paradoxically seems to follow the increases and decreases of outflow, careful examination of the figures shows that sudden drops in outflow create higher water levels. One must also remember that the natural pattern is of minimum flow in winter, rising to a maximum in summer.

In springtime, the role of the Moses-Saunders Dam in controlling outflow is more complex than in January. Sudden changes in water level can be used to collapse or break ice cover in Lake St. Lawrence, but there is also the risk of jamming the ice against the dam, decreasing outflow considerably.

Icebreakers are also used to control the removal of ice in spring. Generally, they are used to clear ice in the immediate vicinity of locks, but they also cut paths as they travel upstream to the next structure. However, there is no evidence from field observations or from aerial photographs that the passage of a single ship through a low velocity area like Lake St. Lawrence speeds breakup of that ice cover.

4.2 Model Testing Site and Time Period

In developing a simulation model, the ideal method of evaluating its performance is to apply it first to a calibration period for optimizing any empirical functions and then to a separate time period to validate its use. The decision was made, however, to limit the initial evaluation to a period for which there are reliable meteorological data from a site located at the river's edge. These data were collected during winter 1975-76 at a small meteorological station installed in August, 1975, for the St. Lawrence Seaway Development Corporation. Although the system is currently being improved, former problems with sensor maintenance allow only the first winter's data to be used reliably.

Meteorological input data for the simulation models were provided by sensors located at this same station, on a pier projecting into the river at Ogdensburg. The instruments are located on a tower roughly 10 m above summer water levels and rising 3 m above the roof level of the warehouse supporting the tower. A paper tape punch and a line printer located inside the warehouse record the hourly observations of air temperature, vapor pressure, wind speed, and atmospheric pressure. Shortwave radiation incident on a horizontal surface was accumulated for a 24-h period and reset to zero at midnight. Mean daily averages from these observations for the period from September 1975 to August 1976 are listed in appendix E. Table 3 lists the sensors and their accuracy.

In addition to the meteorological parameters, mean daily river water temperature is needed by the models. Daily readings are available for this time period at two locations. The first is located 3 m below the surface (10-m water depth) at a ship loading dock near Waddington. A second set of temperatures is taken at the intake gates of the Moses-Saunders Dam at Cornwall.

TABLE 3.--*Meteorological sensors at Ogdensburg station*

Variable	Sensor	Accuracy
Air temperature	Platinum resistance thermometer in radiation shield.	+1°C
Vapor pressure	Lithium chloride dew cell in radiation shield.	Less than 5% when > 0°C. More than 10% when < -20°C.
Wind speed	3-cup anemometer (3.0 m s ⁻¹ threshold).	The larger of 10 cm s ⁻¹ or 2%.
Shortwave radiation	Eppley precision pyranometer.	2%

In order to give a quantitative check of the model performance, ice thickness data is also needed. This information has been gathered by the St. Lawrence Seaway Authority (SLSA) in Cornwall at 28 sites along the ship channel between Montreal and Lake Ontario for every winter since 1971.

Figure 5 shows eight stations (with their St. Lawrence Seaway Authority identification) in the vicinity of Ogdensburg and Lake St. Lawrence. These sites were chosen as potential points of model verification given the location of the input data sensors. Table 4 lists the observed thickness values for the 1975-76 winter and notes those sites where ice thickness measurements were terminated by icebreaker passage. The observations in table 4 are shown graphically in figure 8.

A description of each station and its 1976 ice pattern should help to clarify the variety of ice decay mechanisms on the river. All stations are located in the middle of the shipping track or approximately over the deepest portion of a cross section.

Station F-1 is located in the middle of Lake St. Lawrence, roughly 21-km upstream from the Moses-Saunders Dam. Currents are slow in this section of the river (no more than 1.0 m s⁻¹). Few if any pools occur in this section of

TABLE 4.--Observed ice thickness (cm), upper St. Lawrence River, winter 1975-1976

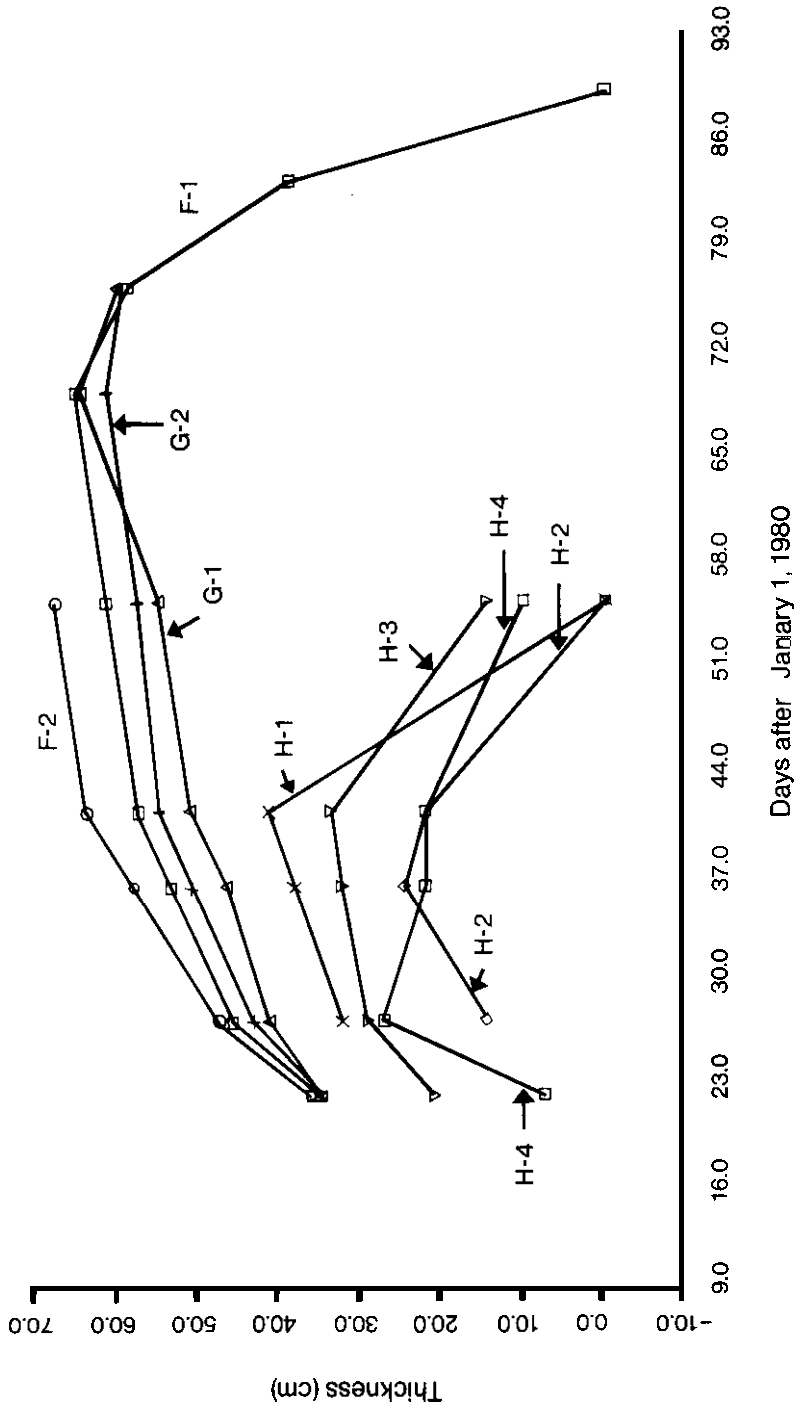
station	Julian Date 1976								
	22	27	36	41	55	69	76	83	89
F-1	34.9	45.7	53.3	57.1	61.0	64.8	50.4	38.7	Open water
F-2	36.2	47.6	57.0	63.5	67.3	Unstable ice, pool nearby		Ice floes	
G-1	34.9	41.3	46.4	50.8	54.6	64.1	59.7	Icebreaker	
G-2	34.3	43.2	50.8	54.6	57.1	61.0	59.1	Icebreaker	
H-1	No obs	32.4	38.1	41.3	Open water				
H-2	No obs.	14.6	24.0	22.2	Open water				
H-3	21.0	29.2	32.4	33.7	14.6	7.6 cm ice broken by icebreaker			
H-4	7.6	27.3	22.2	22.2	10.2				

the ice cover, and it is the only site to thaw in place with very little mechanical action. Both this station and the next, F-2, are shown in figure 9.

Station F-2 is located at the downstream tip of Ogden Island in a region known for its mid-winter hanging ice dams created by trapped frazil ice. As a result of the faster currents in this area and the highly irregular under-ice topography, open water pools frequently occur, as noted in table 4. While a current faster than that at F-1 should produce thinner ice than that found at F-1, it is possible that an insulating layer of frazil (observed frazil thickness was around 60 cm), isothermal at 0°C, allowed more rapid growth to occur.

Both stations G-1 and G-2 are located just upstream of the Iroquois Dam (usually left open in winter) in the narrow stretch of the upper St. Lawrence River. Growth patterns were quite similar to station F-1, but an ice breaker operating out of Iroquois, Ont., prevented observation of the decay pattern.

Station H-1 is located roughly 1-km upstream from G-2, but showed a much different growth pattern. The ice was opened quite early by the downstream growth of the large pool that usually forms on the north side of Galop Island.



8.--Observed ice growth in the upper St Lawrence River, 1975-76.

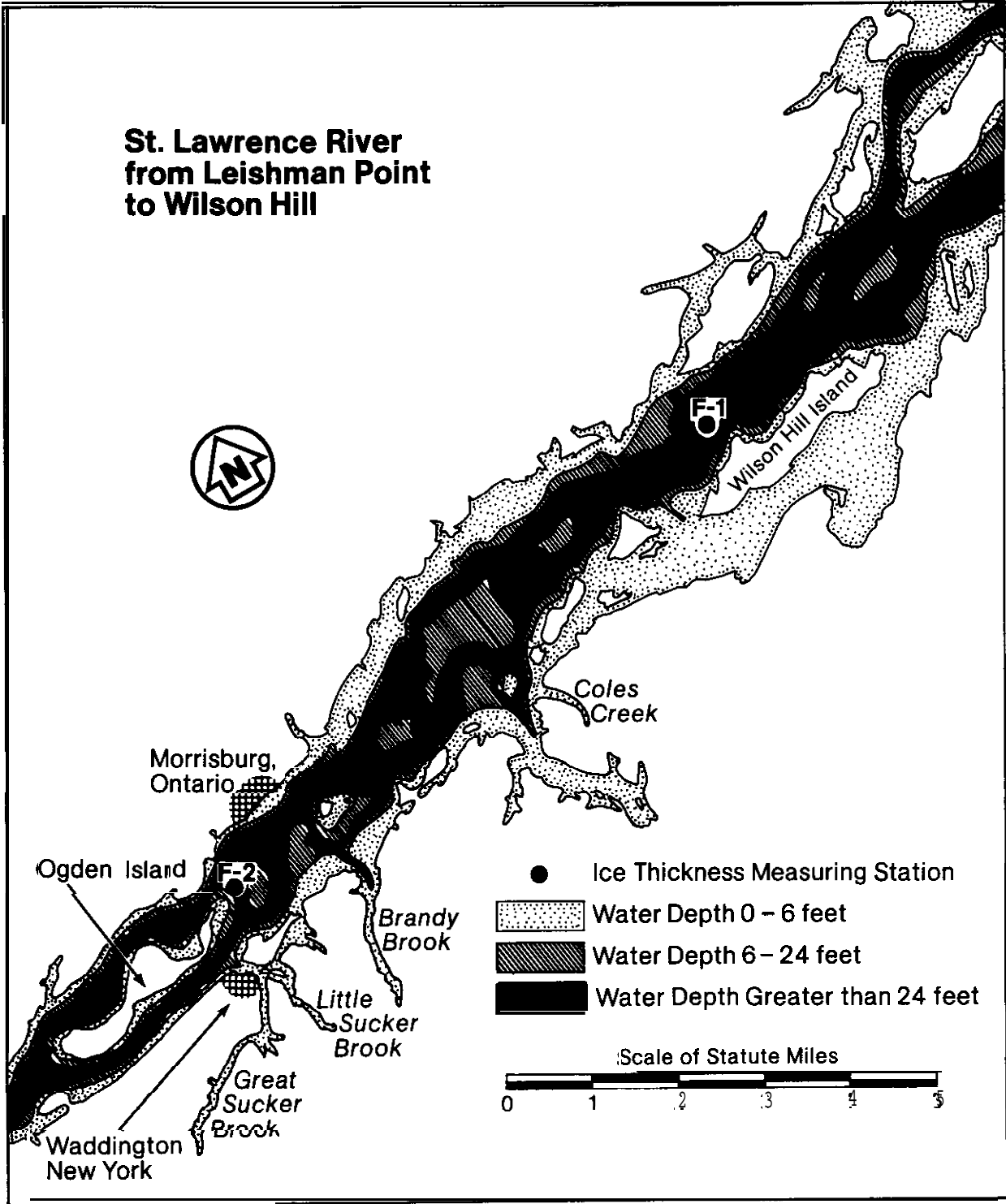


FIGURE 9.--St. Lawrence River from *Leishman Point* to *Wilson Hill Island*.

Station H-2 is upstream of Galop Island, but had a pattern similar to that at H-1; the ice "as thawed by the encroachment of an upstream pool. Ice growth "as only about 50 percent of that at H-1.

Stations H-3 and H-4 are both located upstream of the Ogdensburg-Prescott boom. Ice here "as much thinner than that found at the F and G stations, probably because of the warmer water temperature. Note that the time of maximum ice thickness "as about 1-month earlier than that shown for the F and G stations.

Given the form of these patterns, it "as decided to use observed thickness values at station F-1 for model testing. While stations H-4 and H-3 occur in stable ice areas, their distance from the Waddington or Moses-Saunders water temperature sensors precluded their use. Stations F-2, H-2, and H-1 all were in areas subject to migrating or growing open water pools, and thus it would have been difficult to include them in the model. Given the input data available, stations G-1 and G-2 would be the best sites for modeling. Given that their pattern and overall thickness were similar to those at F-1 before icebreaking, the observed results from Lake St. Lawrence are considered to be comparable.

4.3 Weather and Ice Conditions, Winter 1975-76

Because the model has been tested only over winter 1975-76, it is important to place the weather and ice conditions in the context of the general climatology. Although long term data have not been analyzed for Ogdensburg, comparisons of the 1975-76 winter can be made for Kingston, 105-km upstream.

Figure 10 shows accumulated freezing degree-days for the period 1970-79 (adapted from Assel, 1980). The five severity classes were derived from 80 years of record. The two extremes each represent 5 percent of the observed winters. The next two classes each include 15 percent of the winters, while the "normal" class includes 60 percent of the cases. Accumulated freezing degree-days for the 1976 winter at Kingston totaled 735, placing that winter in the "normal" class. 740 freezing degree-days accumulated at the Ogdensburg meteorological site during the same period, suggesting that the air temperatures at the simulation site were also close to normal. Figure 11 shows the daily trend of air temperatures and Waddington water temperature during this period.

During this winter period, 33.3 cm of water fell as snow at Massena Airport, a departure of 10.2 cm above normal (35 years of record). Over the same period at Ogdensburg Airport, 65-km upstream, 15.7 cm of water fell as snow, a departure of 6.8 cm below normal (84 years of record). No direct measurements of snow fall thickness or density were recorded. The last snowfall at both sites occurred on March 19. Between that snowfall and the observed absence of ice on March 30, 1.5 cm and 1.7 cm of rain fell at Massena and Ogdensburg, respectively.

Ice conditions, however, appeared to be somewhat more severe than normal. According to the Navigation Season Extension Study report for 1975-76:

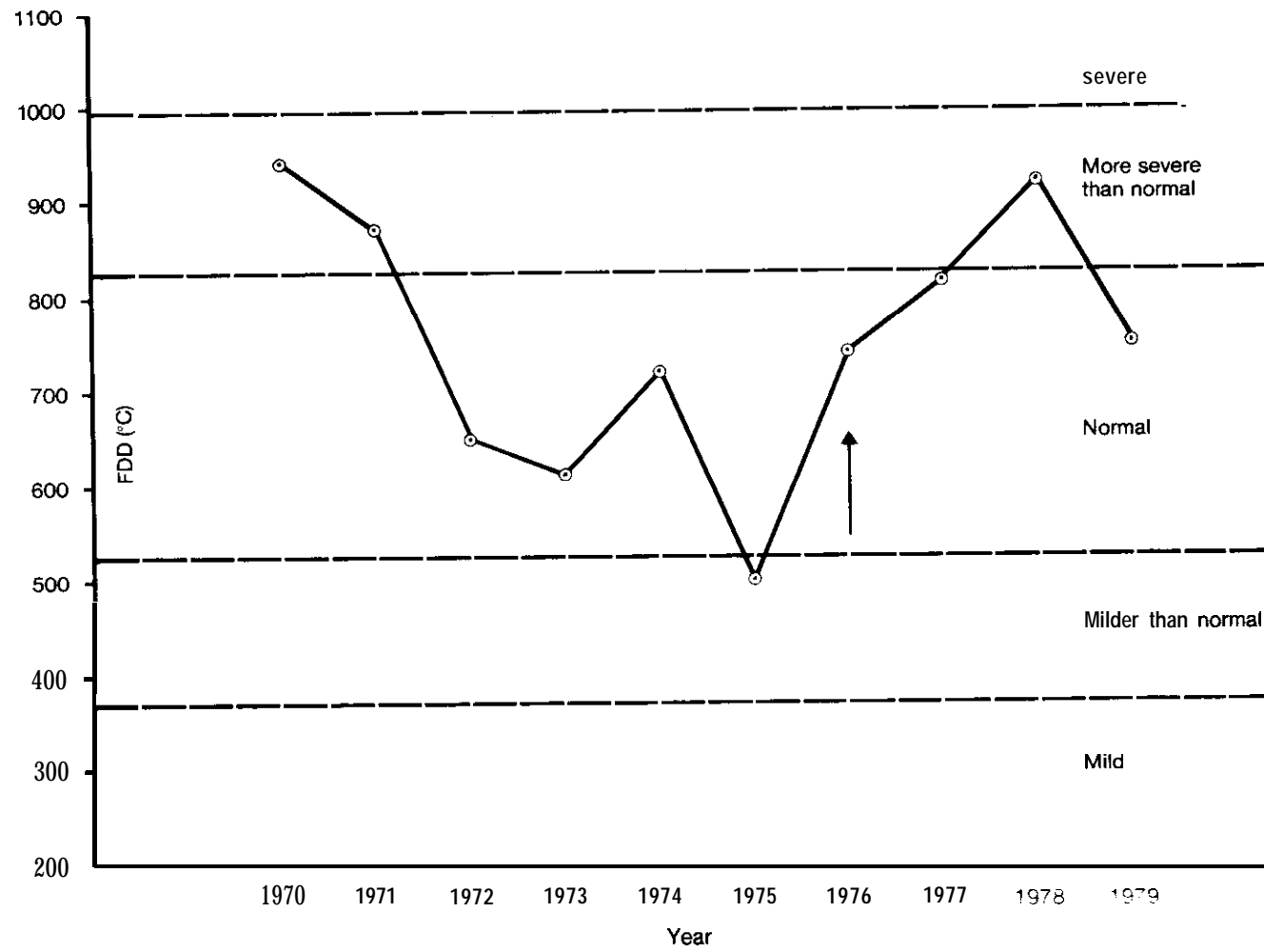


FIGURE 10.--Winter severity at Kingston, Ont., 1970-79.

DAILY AIR TEMPERATURE AND WATER TEMPERATURE

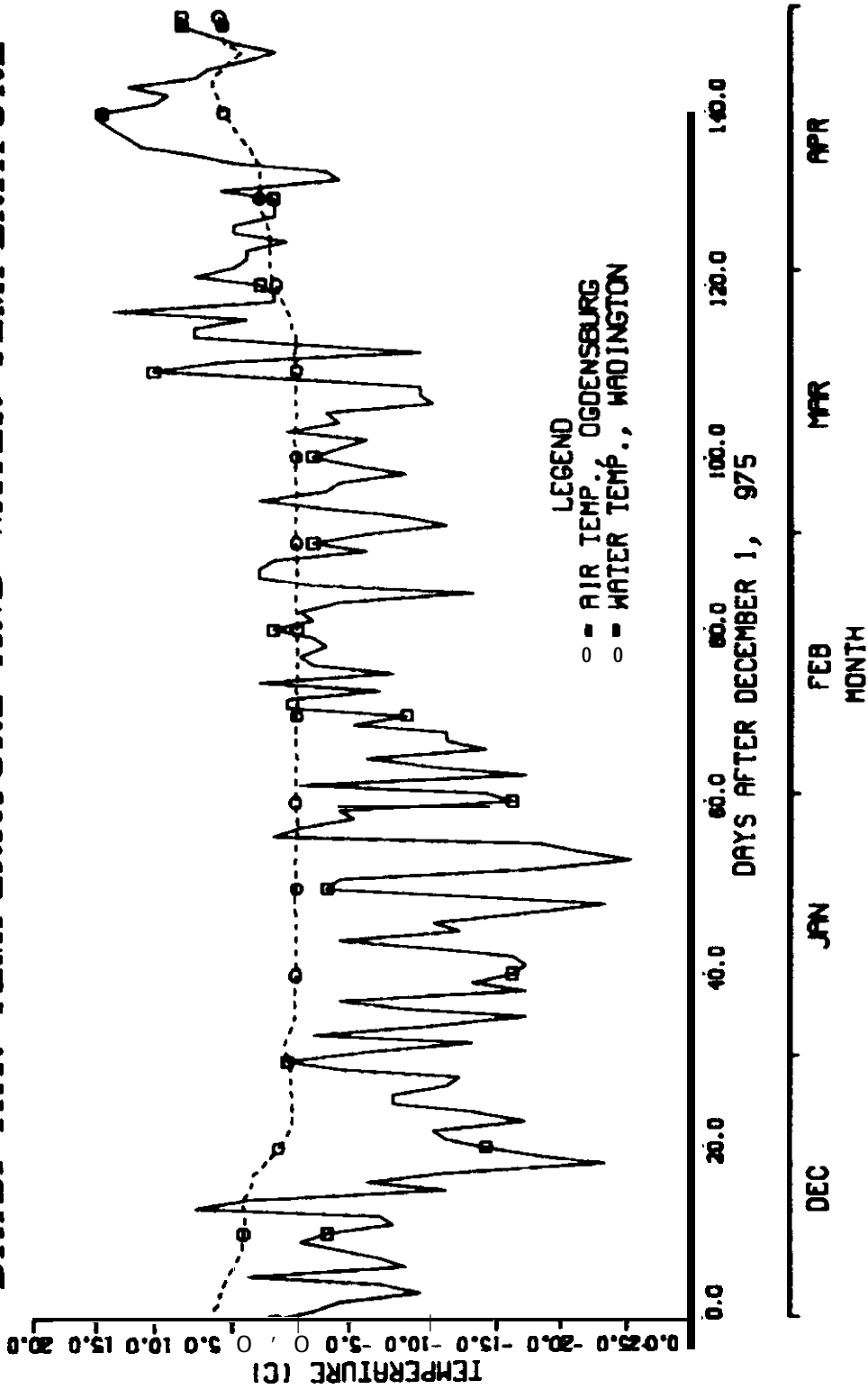


FIGURE 1.1 - Daily air and water temperatures, upper St Lawrence River, 1975-76.

Winter ice cover had formed by December 19, 1975, in the South Shore Canal, Montreal, and advanced upriver to Lake Ontario by January 18. Ice conditions during mid-winter were more severe than the previous three winters, being generally compared to 1972. However, due to unusually mild weather, which persisted throughout the last week of March and early April, the ice cover deteriorated very quickly and the river was almost entirely ice free by April 2.

As determined from aerial photographs of the river, complete ice cover formed in the Wilson Hill area between January 8, when the water was 50 percent filled with ice floes, and January 12, when the ice cover became solid. Likewise, breakup took place between March 26, when a solid cover was still in place, and March 30, when the area was open water. Table 5 shows how these dates compare to the eight winters between 1972-79. Note that breakup date and maximum ice thickness are not well correlated. For example, both the 1975 and 1977 breakup occur at the same time, but the 1977 maximum ice cover was almost twice as thick.

4.4 Simulation Results

4.4.1 Analytic Models

As described in the discussion of models, three analytic models were used to simulate ice growth. Using wind speed and air temperature from Ogdensburg and the average of the Waddington and the Moses-Saunders stations for water temperature, the simulation results were matched against observed ice thicknesses at Wilson Hill. The results are shown in figure 12. The uppermost curve represents the theoretically maximum amount of growth as predicted by the Stefan solution to equation (28) when no snow is present. If snow is allowed to accumulate up to the maximum of 8 cm observed on the ice, then equation (32) can be applied ("TA = TS, SNOW").

The third approach was to allow turbulent transfer to take place between ice and the atmosphere by applying equation (34) ("TA NOT = TS, SNOW"). This curve most closely matches the observations. With snow, the Stefan solution first overestimates and then underestimates growth.

All three of these ice growth relations were derived for lake ice with no underice turbulent transfer. The good approximation of the models to ice growth in this area is not surprising given the lake-like characteristics in this reach of the river created by the Moses-Saunders Dam.

As figure 8 illustrates, however, other reaches of the river develop much less ice. For example, the reach of river upstream from Ogdensburg, narrower and with faster currents, had ice only half as thick as that in Lake St. Lawrence. Michel's suggestion (1971) of the use of a factor in equation (30) to adjust the Stefan solution to river conditions is also followed in figure 12. The lowest curve represents the theoretical maximum times a factor of 0.5, which Michel suggested for an "average river with snow." The resulting values roughly match observations taken at station H, just upstream from Ogdensburg.

TABLE 5.--Breakup dates, *Wilson* Hilt Island, 1972-79

Year	Last evidence of ice cover (Julian date)	First evidence of no ice cover (Julian date)	Maximum thickness (cm)
1972	103	111	62
1973	66	73	37
1974	65	67	52
1975	78	80	36
1976	86	90	65
1977	77	81	70
1978	89	96	68
1979	80	87	61
Mean	80.5	85.6	56.4
Standard deviation	12.4	13.8	13.4

Breakup evidence from aerial photographs and Navigation Season Extension Studies.

Ice thickness from data provided by the St. Lawrence Seaway Authority.

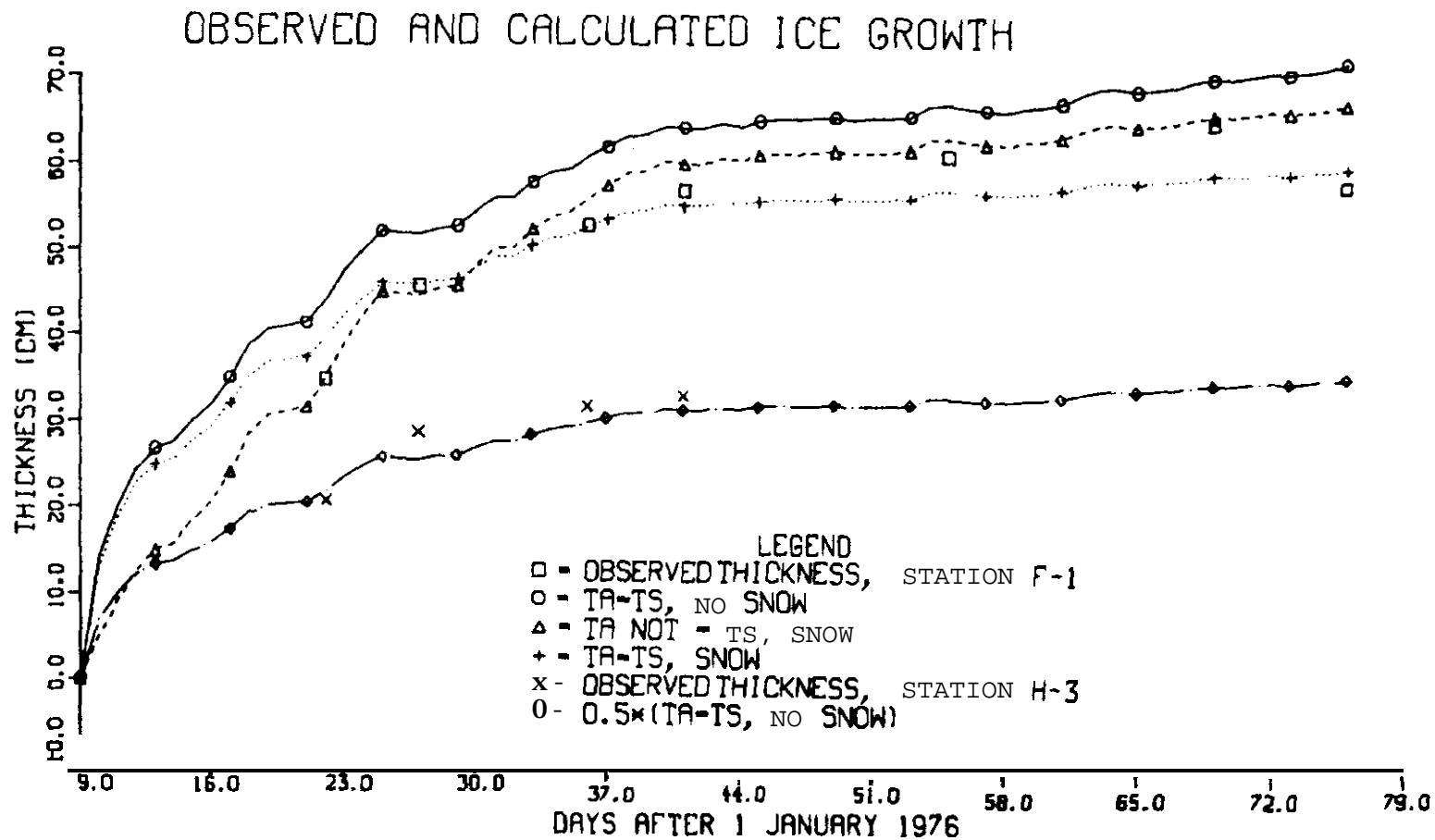


FIGURE 12.--Ice growth simulated by analytic models.

The first approach to simulating ice decay incorporates equation (36) into a step-wise solution. Figure 13 compares the results of this simulation with observations at station F-1 adjacent to Wilson Hill Island. Estimating the current as 50 cm s⁻¹, the depth as 20 m, and starting with the observation of 65 cm of ice on March 9, the model predicts the loss of all ice 2 days prior to the first day no ice was observed.

Such results appear respectable given the assumptions used in the application of the melt model to this site. Air temperatures from Ogdensburg were assumed equal to those experienced at Wilson Hill. The water temperature used was the average of the Waddington and the Moses-Saunders Dam temperatures. Finally, there is a 7-day gap between the observation of 65 cm of ice on March 9 and the next observation of 58 cm of ice on March 16. It is assumed that the maximum thickness was that observed on the 9th.

Ashton's work (1978) has shown that the underice formation of ripples during spring melt increases the effective turbulent transfer of heat. He points out that B_1 may need to be increased by 50 percent to adequately simulate melt. The lowest curve in figure 13 shows the results of using a B_1 enlarged by 50 percent from plane surface values. This change speeds the melt out of the ice layer by 4 days.

The Ashton decay model was also tested in a faster stretch of the river above Ogdensburg. Spring currents in this area have been estimated at 150 cm s⁻¹. Observations at station H-3 showed 34 cm of ice on February 10, decreasing to 15 cm on February 24. The model estimated much quicker decay, showing complete melt by February 17. It is unknown, however, how significantly water temperatures at H-3 vary from those measured at Waddington, 32-km downstream.

4.4.2 Energy Balance Model

Figure 14 shows the result of applying the energy balance model to the 1975-76 winter period at station F-1 near Wilson Hill Island. The model was started with 4 cm of ice on January 9 and then was driven by the Ogdensburg meteorological data. The simulated thickness increased by 20 cm within 5 days, but steadily slowed its rate of growth as the winter progressed and the ice thickened. The simulated ice decay is sudden, dropping from a maximum of 48 cm on day 85 to 0 cm on day 89, corresponding to the midpoint of the period when ice actually left this stretch of the river.

Figure 15 plots the observed air and the simulated ice surface temperatures over the same period. The significant result to note in this figure is the increased coupling between surface and air temperatures as the ice thickens. Whereas temperature differences of up to 14°C are shown in mid-January, this difference does not exceed 5°C in March, when the ice thickness is 42 cm or thicker (except when air temperature is above 0°C).

The two principal limitations of the simulated results are that the simulated maximum ice thickness is only 75 percent of the observed thickness. In addition, the simulated time of maximum thickness lags the observed time by 2 weeks. Consequently, the simulated ice decay is much more abrupt than that observed.

OBSERVED AND CALCULATED ICE DECAY, STATION F-

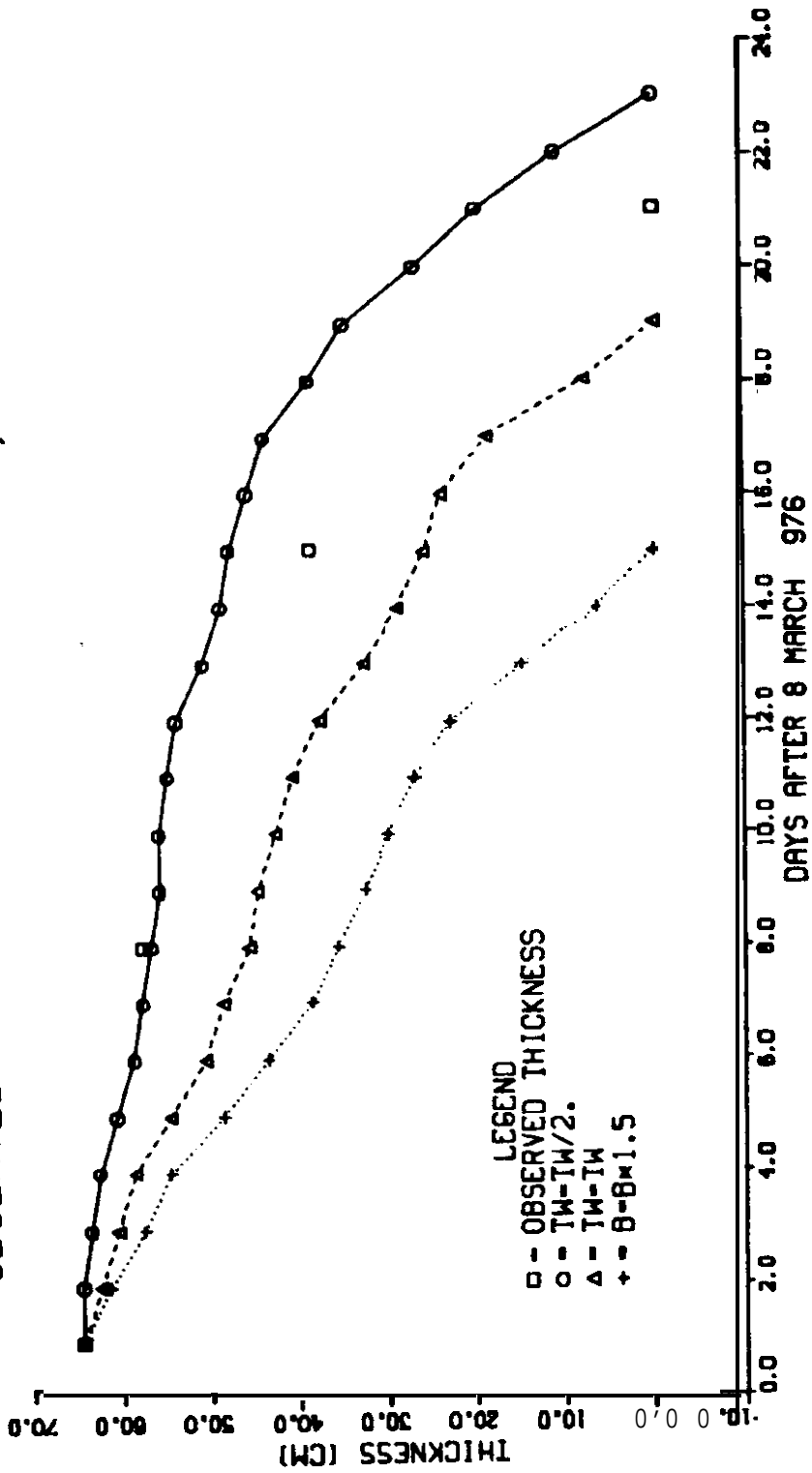


FIGURE 13. -Ice decay simulated by analytic model.

SIMULATED ICE THICKNESS, STATION F-1

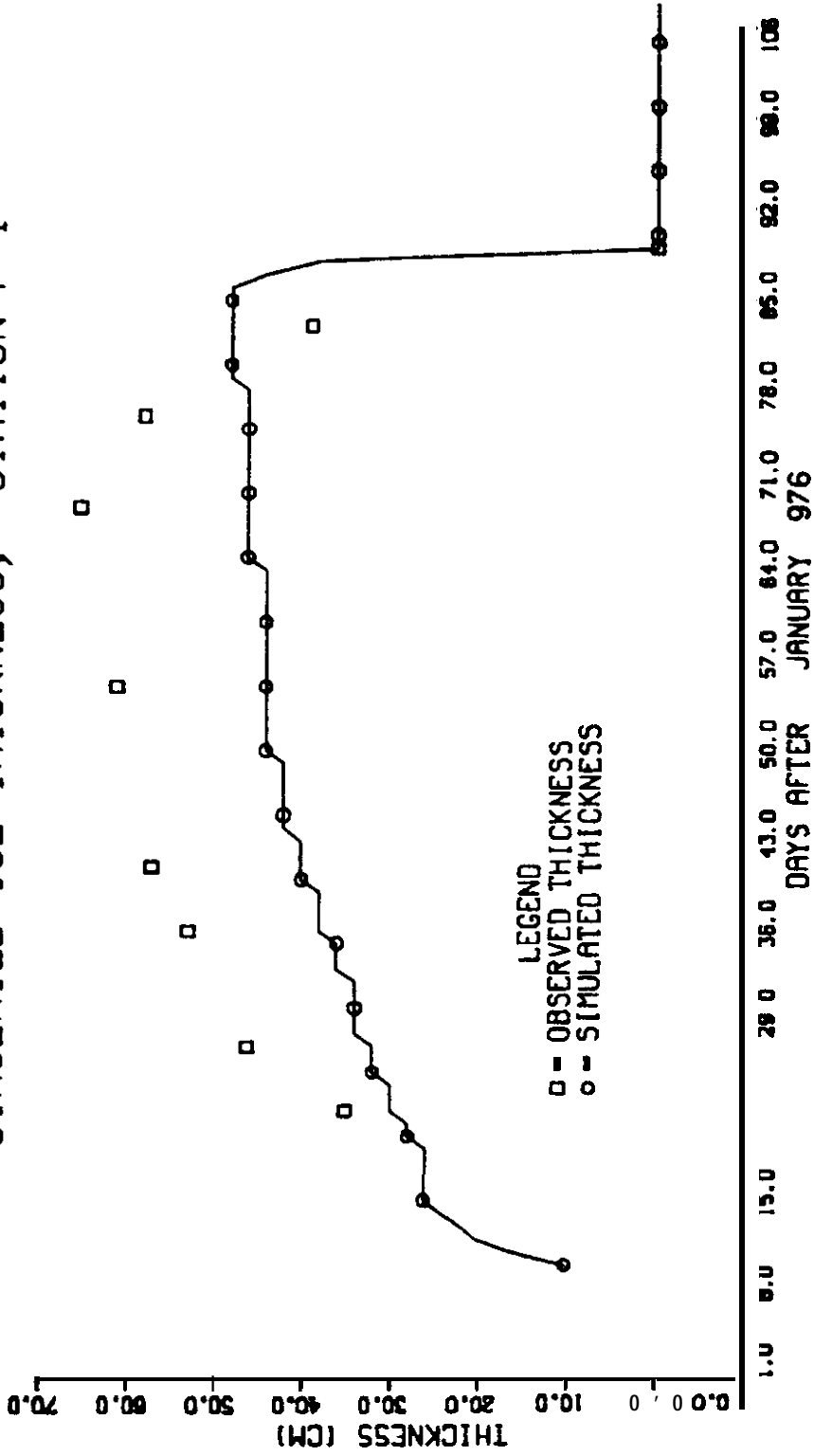


FIGURE 14.- Ice growth and decay simulated by energy balance model with 2-cm node spacing

AIR TEMP. AND SIMULATED ICE SURFACE TEMP.

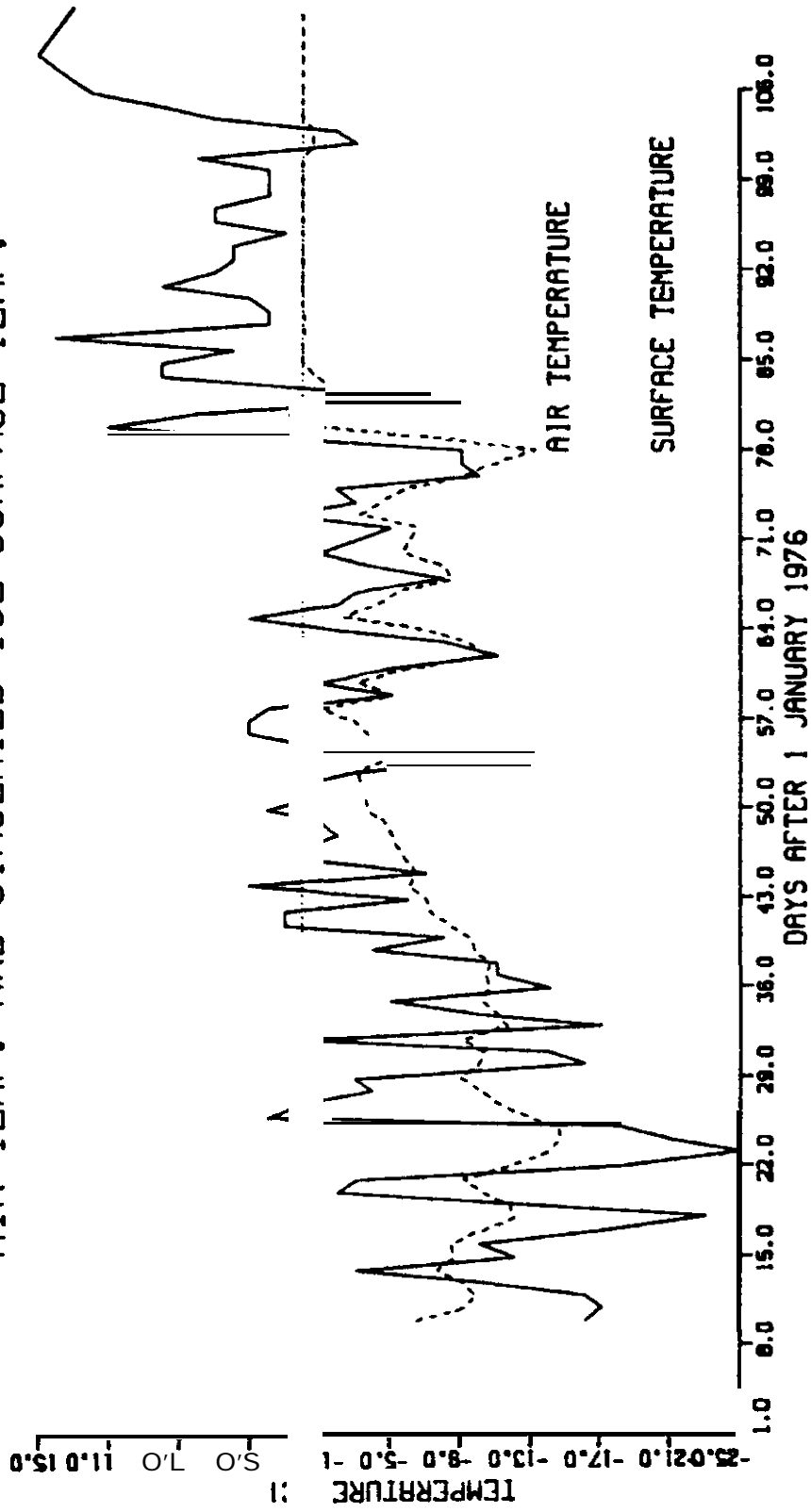


FIGURE 15 -Surface temperature simulated by energy balance model with 2-cm node spacing.

Special note should be made of the sensitivity of the model to computation node spacing, Z_n (figure 2). When node spacing was decreased from 2 cm to 1 cm, maximum ice thickness dropped from 40 cm to 38 cm. When node spacing was increased to 4 cm, the maximum ice thickness produced was 60 cm. Figure 16 shows the simulated growth and decay pattern when the node spacing is 4 cm. Comparison with figure 14 shows that the greatest difference occurred within the first week of growth, suggesting that the model did not adjust well to the initial conditions. Despite the greater thickness, a node spacing of 4 cm was not considered for the standard runs because the model growth exceeds the theoretical maximum shown in figure 13 for the first few weeks.

Table 7 shows that the simulated breakup date was less responsive to variation in model parameters than was simulated maximum ice thickness. The four most significant variables are the same as in table 6, with one exception. Snow-cover thickness, Z_s , has replaced water temperature as the third most important variable. This may appear surprising until one realizes that solar penetration is the major influence in the rate of ice decay in the model. In the model, shortwave absorption within the ice occurs only after the snow layer has melted. For example, as indicated in figure 16, the decay of 60 cm of ice required only 2 days longer than the decay of 48 cm of ice.

As indicated in table 7, a water temperature variation of $+0.5^\circ\text{C}$ (with a lower limit of 0.01°C) had no effect on the breakup date. Such a result is clearly unrealistic, but is possible with the model because Q_w , turbulent transfer between the ice and water, was not included.

5. DISCUSSION

As shown by the description of ice conditions found on the upper St. Lawrence River, there is considerable variation in the influence of energy and mass transfer processes on ice cover. The growth curves in figure 8 illustrate, however, that there are two general patterns of growth and decay: those associated with regions of slower currents with stable ice cover and those with regions of faster currents with either stable or unstable ice cover.

Examination of figures 12 and 13 shows that simulations based solely on changes in air and water temperatures produce reasonable simulations of observed ice thicknesses and breakup dates. The addition of a snow cover or turbulent transfer mechanisms in the air made relatively little difference in the simulation results.

In faster stretches of water, the addition of an empirical factor that acknowledges the increasing influence of turbulent transfer with the water allows growth to be accurately simulated. However, in these stretches, the analytical method simulated ice decay at a rate much faster than actually observed. One problem may have been the use of water temperature data from a site 32-km away. Ashton (1978) and Ashton and Kennedy (1970) have emphasized the influence of very small temperature variations on the rate of melt.

SIMULATED ICE THICKNESS, WILSON HILL

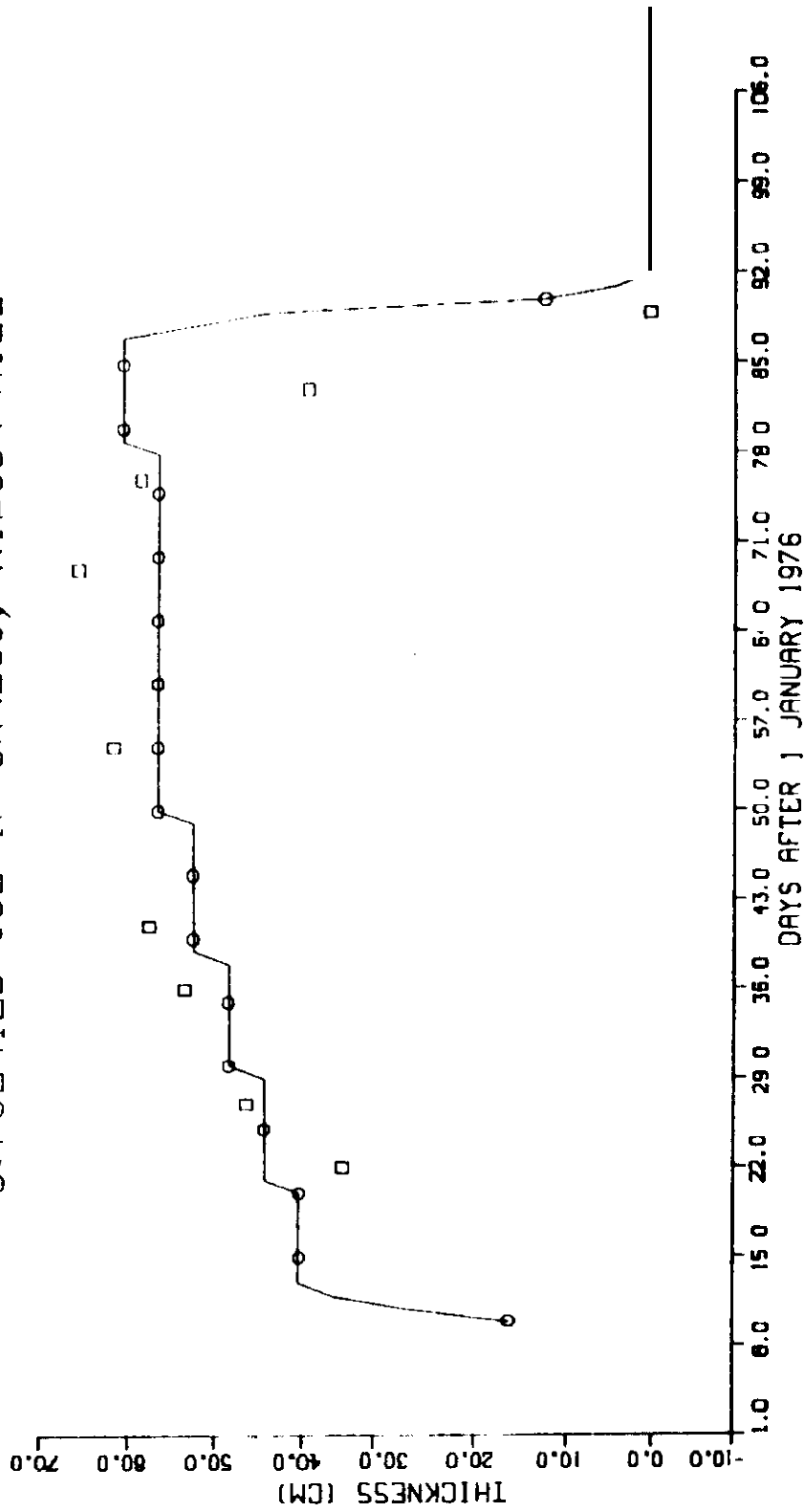


FIGURE 16. -Ice growth and decay simulated by energy balance model with 4-cm node spacing

TABLE 7.--Sensitivity analysis for energy balance model,
date of breakup

	Sensitivity	Relative importance
T_a ($^{\circ}\text{C}$)	3.90	1.40
Q_{rnl} (W m^{-2})	0.06	0.34
Z_s (m)	1.35	0.21
Q_{sw} (W m^{-2})	0.04	0.15
T_d ($^{\circ}\text{C}$)	0.22	0.07
U (m s^{-1})	0.00	0.02
T_w ($^{\circ}\text{C}$)	No effect	
A (1%)	0.22	0.07
Z_o (cm)	3.12	0.01
vK	No effect	
Cl	2.25	0.07
Z_n (cm)	0.85	0.02

As discussed previously, the surface energy balance model was applied to only one site on the river, a region with relatively little current. **For** this reason, turbulent heat exchange between the ice and water was not included in the model. Consequently the ice growth simulated in figures 14 and 16 continued past the observed time of maximum thickness. However, the **internal absorption** of shortwave radiation after the snow layer has melted quickly melts the ice.

One process ignored by the analytic models is the formation of snow ice. Measurements made at stations F-1 and F-2 during the 1975-76 winter show that snow ice formed the upper 40 percent of the ice cover by the time of maximum thickness. As Adams and Roulet (1980) have shown, snow **cover** can either inhibit ice growth because of its insulating properties or accelerate growth when cracking occurs and the snow becomes saturated.

In the energy balance model, this effect was adjusted for by allowing only the observed maximum snow depth to accumulate; that is, even though more than 150 cm of snow fell during winter, the snow layer in the model built up to only 8 cm, the maximum amount observed. In this way, the rhythm of ice growth deceleration and acceleration caused by snow falls and their subsequent saturation are smoothed **over** by the model.

As discussed previously, the equations used in the analytic models essentially simulate only the heat conduction and **longwave** radiation exchange processes. Turbulent transfer and shortwave radiation flux are ignored. Sensitivity analysis of the energy balance model, however, suggests that heat conduction and net **longwave** radiation are the most significant **processes**.

6. CONCLUSIONS

The general question guiding this report has been, "To what extent can ice decay on the upper St. Lawrence River be simulated?" Two general types of models have been constructed and applied to the river **over** the 1975-76 winter. Analytic growth models based on the assumption of a linear temperature gradient through the ice agreed closely with observed ice thickness. Addition of snow cover or turbulent heat exchange with the air made relatively little difference in the simulation results. An analytic melt model produced a good approximation of ice thickness and the breakup date in the lake-like stretches of the river but not in the faster reaches where turbulent heat exchange between the ice and water would be more significant.

The other type of model tested was a surface energy balance model, which couples analysis of each of the relevant energy fluxes with a finite difference temperature diffusion scheme. While this model accurately simulated breakup dates in a slow current stretch of the river, it underestimated maximum ice thickness. Ice decay was essentially a thermodynamic process, including loss of ice at both the upper and lower surfaces and the internal absorption of shortwave radiation. Given the success of a model incorporating only these **processes**, it was not necessary to allow for either turbulent exchange with the water or for mechanical destruction of the ice cover.

Results from these models clearly indicate the direction of future work. Despite the apparent accuracy of the analytic models, their simplicity limits the amount of probing that can be done into the key processes of **longwave** and shortwave absorption and turbulent heat transfer between the water and the ice **cover**. A surface energy balance model that incorporates that turbulent transfer will **more** accurately portray the coupling of surface and underwater processes. (Results of this modification are presented in Green, (1981).)

Such a model would also benefit from additional studies of water temperature and radiation along the river. For example, water temperature sensors at Kingston, and at the Moses-Saunders Power Dam show little or none of the expected temperature drop over the 170 km between them. Is this caused by sensor accuracy, location, or additional sources of heat for the river water?

On a larger scale, the heterogeneity of the ice cover in the vertical direction needs to be considered because of its effects on both the transfer of heat and the absorption of shortwave radiation. The energy balance model already has this capacity, but lacks meaningful data from the river for verification.

The sensitivity analysis demonstrated the significance of air temperature and the radiation fluxes. In order to extend verification of the models to other years, it would be necessary to compare data from other sites near the river (e.g., Kingston, Montreal, **Massena**) with the Ogdensburg riverside site. If these variables are well correlated over the winter period, it will be possible to test a greater range of ice seasons.

7. ACKNOWLEDGMENTS

I gratefully acknowledge the support of the St. Lawrence Seaway Development Corporation and the St. Lawrence Seaway Authority. Both provided data used to test and apply the simulation model. Steve Hung in particular, at the Washington office of the St. Lawrence Seaway Development Corporation, was very generous in providing the Ogdensburg meteorological data and information on the operation of the seaway. Much of the theoretical work on the surface energy balance model was done with the support of Dr. Samuel **Outcalt** at the Department of Geography, the University of Michigan.

A portion of the work was funded under the auspices of the Great Lakes-St. Lawrence Seaway Navigation Season Extension Program.

8. REFERENCES

- Acres American, Inc. (1978): Water levels and ice modeling studies. In: **Environmental Assessment of the FY 79 Winter Navigation Demonstration on the St. Lawrence River**, State University College of Environmental Science and Forestry, Syracuse, N.Y., pp. E1-E68.
- Adams, C. E. (1976): Estimating water temperatures and time of ice formation on the St. Lawrence River. *Limnol. Oceanogr.* **21:128-137.**
- Adams, W. P., and Roulet, N. T. (1980): Illustration of the roles of snow in the evolution of the winter cover of a lake. *Arctic* **33:100-116.**
- Anderson, E. A. (1976): A point energy and mass balance model of a snow cover. NOAA Technical Report, NWS 19. U.S. Department of Commerce, Washington, D.C.
- Anderson, E. A. and Baker, D. R. (1967): Estimating incident terrestrial radiation under all atmospheric conditions. **Water Resour. Res.** **3:975-988.**
- Antonov, V. S., Ivanov, V. V., and Nalimov, Y. V. (1973): Types of breakup of rivers in Siberian Arctic and sub-Arctic zones. In: Proceedings Symposium on the *Role of Snow and Ice in Hydrology*, International Association for Hydrological Sciences, Banff, Alb. September, 1972, pp. 541-546.
- Ashton, G. D. (1973): Heat transfer to river ice covers. In: **Proceedings Eastern Snow Conference**, pp. 125-135. (Available from Cold Regions Research and Engineering Laboratory Library, Hanover, N.H.)
- Ashton, G. D. (1978): River ice. *Ann. Rev. Fluid Mech.* **10:369-392.**
- Ashton, G. D. (1979) Suppression of river ice by thermal effluents. CRREL Report 79-30. Cold Regions Research and Engineering Laboratory, Hanover, N.H., 26 pp.
- Ashton, G. D. and Kennedy, J. F. (1970): Ripples on underside of river ice covers. *J. Hydraul. Div.*, ASCE **98:1603-1624.**
- Assel, R. A. (1980): Maximum freezing degree-days as a winter severity index for the Great Lakes 1897-1977. *Monthly Wea. Rev.* **108:1440-1445.**
- Barnes, H. T. (1906): **Ice Formation**. John Wiley and Sons, New York, 257 pp.
- Beckett, R., and Hurt, J. (1967): **Numerical Calculations and Algorithms**. McGraw-Hill, New York, 295 pp.
- Bilello, M. A. (1980): Maximum thickness and subsequent decay of lake, river, and fast sea ice in Canada and Alaska. CRREL Report 80-6. Cold Regions Research and Engineering Laboratory, Hanover, N.H., 165 pp.

- Bolsenga, S. J. (1967): Total atmospheric water vapor aloft over the Great Lakes basin. Research Report 5-3. U.S. Lake Survey, Detroit, Mich.
- Bolsenga, S. J. (1977): Preliminary observations of the daily variation of ice albedo. *J. Glaciol.* 18:517-521.
- Bulatov, S. N. (1973): Computation of the strength of the melting ice cover of rivers and **resevoirs** and forecasting the time of its erosion. In: **Proceedings, Symposium on the Role of Snow and Ice in Hydrology**, International Association for Hydrological Sciences, Banff, Alb., September 1972, pp. 575-581.
- Businger, J. A., Wyngaard, J. C., Izumi, Y., and Bradley, E. F. (1971): Flux profile relationships in the atmospheric surface layer. *J. Atmos. Sci.* 28:181-189.
- Carstens, T. (1970): Heat exchange and **frazil** formation. In **Proceedings Symposium on Ice and Its Action on Hydraulic Structures**, International Association for Hydraulic Research, Reykjavik, Iceland, September 1970, pp. 117-124.
- Coleman, G., and DeCoursey, D. G. (1976): Sensitivity and model variance analysis applied to some evaporation and evapotranspiration models. *Water Resour. Res.* 12:873-879.
- Dingman, S. L., Weeks, W. F., and Yen, Y. C. (1967): The effect of thermal pollution on river ice conditions--A general method of calculation. CRREL Research Report 206. Cold Regions Research and Engineering Laboratory, Hanover, N.H.
- Dingman, S. L., Weeks, W. F., and Yen, Y. C. (1968): The effect of thermal pollution on river ice conditions. *Water Resour. Res.* 4:349-362.
- Dybig, W. (1977): The computer simulation of mass and heat transfer in a one-dimensional snowpack. Unpublished Master of Science Thesis. Department of Agricultural Engineering, University of Saskatchewan, Regina, Sask.
- Dyer, A. J. (1974): A review of flux-profile relationships. *Boundary Layer Meteorol.* 7:363-372.
- Greene, G. M. (1981): Simulation of ice-cover growth and thermal decay on the upper St. Lawrence River. Ph.D. dissertation. Department of Geography, University of Michigan, Ann Arbor, Mich., available from University Microfilms, Ann Arbor, Mich. 165 pp.
- Ince, s., and Ashe, G. W. T. (1964): Observations on the winter temperature structure of the St. Lawrence River. In: **Proceedings, 21st Eastern Snow Conference**, Utica, New York, pp. 1-13. (Available from Cold Regions Research and Engineering Laboratory Library, Hanover, N.H.)
- Kerry, J. G. G. (1946): The winter temperature cycle of the St. Lawrence waters. *Eng. J.* 29:26-34.

- Koren'kov, V. A. (1970): Experimental research findings on the decrease of river ice strength in spring. In: **Proceedings, Symposium on Ice and Its Action on Hydraulic Structures**, International Association for Hydraulic Research, Reykjavik, Iceland, September 1970.
- Lowe, P. R. (1977): An approximating polynomial for the computation of saturation vapor pressure. *J. Appl. Meteorol.* **16:100-103.**
- Maguire, J. J. (1975): Light transmission through snow and ice. Technical Bulletin 91. Canadian Centre for Inland Waters. Burlington, Ont., 35 pp.
- Male, D. H. and Granger, R. J. (1978): Energy and mass fluxes at the snow surface in a prairie environment. In: **Proceedings, Modeling of Snow Cover Runoff**, ed. S. Colbeck and M. Bay, Cold Regions Research and Engineering Laboratory, Hanover, N.H., pp. 101-124.
- Marshall, E. W. (1978): Ice survey studies. Environmental assessment of the FY 1979 winter navigation demonstration on the St. Lawrence River. Technical Reports, Vol. II. State University College of Environmental Science and Forestry. Syracuse, N.Y., pp. H1-HV2.
- Marshall, E. W. (1979): Waterfowl, and raptors study, St. Lawrence River, Part II: Glaciology--pool characteristics. Environmental Evaluation Work Group, Winter Navigation Board. U.S. Army Corps of Engineers, Detroit, Mich., 141 pp.
- Maykut, G. A. and Untersteiner, N. (1971): Some results from a time-dependent thermodynamic model of sea ice. *J. Geophys. Res.* **76:1550-1575.**
- Michel, B. (1971): Winter regime of rivers and lakes. Monograph III-B1A. Cold Regions Research and Engineering Laboratory, Hanover, N.H., 130 pp.
- Michel, B. (1973): Properties and processes of river and lake ice. In **Proceedings, Symposium on the Role of Snow and Ice in Hydrology**, International Association of Hydrological Sciences, Banff, Ont., pp. 454-469.
- Michel, B. and R. O. Ramseier. (1970): Classification of river and lake ice. *Can. Geotech. J.* **8:36-45.**
- Outcalt, S. I. (1977): The effect of iteration frequency on a numerical model of near-surface ice segregation. *Eng. Geol.* **13:111-124.**
- Outcalt, S. I., and Carlson, J. H. (1975): A coupled soil thermal regime surface energy balance simulator. In: **Proceedings Conference on Soil-Water Problems in Cold Regions**, Special Task Force, Division of Hydrology, Amer. Geophys. Union., Calgary, Alb., pp. 22-65.
- Outcalt, S. I. and H. Allen (1980): The thermal response of Lake Ohrid, Yugoslavia, to meteorological conditions. In review.

- Philip, J. R. and D. A. DeVries (1957): Moisture movement in porous material under temperature gradients. *Trans., Am. Geophys. Union* **38:222-232**.
- Pivovarov, A. A. (1973): *Thermal Conditions in Freezing Lakes and Rivers*. John Wiley and Sons, New York, 134 pp.
- Quinn, F. H. (1979): An improved aerodynamic evaporation technique for large lakes with application to the International Field Year for The Great Lakes. *Water Resour. Res.* **15:935-940**.
- Sellers, W. D. (1965): *Physical Climatology*. University of Chicago Press, Chicago, Ill., 272 pp.
- Shishokin, S. A. (1969): Investigation of the Bouger-Lambert formula for the penetration of solar radiation into ice. *Soviet Hydrol.: Selected Papers* **3:287-295**.
- Shulyakovskii, L. G. (ed.) (1966): *Manual of ice-formation forecasting for rivers and inland takes, Manual of Hydrological Forecasting 4. U.S.* Department of Commerce, Israel Program for Scientific Translations, Jerusalem, 245 pp.
- St. Lawrence Seaway Authority (1976): Navigation season extension studies, **Montreal-Lake Ontario section, St. Lawrence River, 1975-1976**. Canadian Marine Transportation Administration, Ottawa, Ont. pp. 1-16.
- Weeks, W. F. and S. L. Dingman (1973): Thermal modification of river ice covers, progress and problems. In: **Proceedings, Symposium on the Role of Snow and Ice in Hydrology**, International Association of Hydrological Sciences, Banff, Alb., pp. 1427-1436.
- Williams, G. P. (1963): Heat transfer coefficients for natural water surfaces. In: **Proceedings, International Association of Scientific Hydrology**, Publication No. 62, International Union of Geodesy and Geophysics, pp. 203-212.
- Williams, G. P. (1970): Breakup and control of river ice. In: **Proceedings Symposium on Ice and Its Action on Hydraulic Structures**. International Association of Hydraulic Research, Reykjavik, Iceland, pp. 203-220.
- Witherspoon, D. F. and R. Y. Poulin (1970): A study of the heat loss of the St. Lawrence River between Kingston and Cornwall. In: **Proceedings 13th Conference of Great Lakes Research**, International Association of Great Lakes Research, Ann Arbor, Mich., pp. 990-996.
- Yen, Y-C. (1969): Recent studies on snow properties. In: *Advances in Hydrosience*, Academic Press, N.Y. pp. 173-214.

Appendix A. SYMBOLS

A	Albedo
B	Constant used in equation 8
C	Heat capacity ($\text{J m}^{-3} \text{ }^\circ\text{C}^{-1}$)
c_p	Specific heat of air at constant pressure ($\text{J kg}^{-1} \text{ }^\circ\text{C}^{-1}$)
C_h	Bulk transfer coefficient for sensible heat
C_m	Bulk transfer coefficient for momentum (drag coefficient)
C_w	Bulk transfer coefficient for latent heat
D_h	Eddy diffusivity for sensible heat ($\text{m}^2 \text{ s}^{-1}$)
D_m	Eddy diffusivity for momentum ($\text{m}^2 \text{ s}^{-1}$)
D_w	Eddy diffusivity for latent heat ($\text{m}^2 \text{ s}^{-1}$)
E	Station adjustment term for equation 14
e_a	saturated vapor pressure at T_a (mb)
e_s	Saturated vapor pressure at T_s (mb)
F	Constant used in equation 30, also Fourier modulus
h_a	Heat transfer coefficient from ice to air ($\text{W m}^{-2} \text{ }^\circ\text{C}^{-1}$)
h_i	Heat transfer coefficient from water to ice ($\text{W m}^{-2} \text{ }^\circ\text{C}^{-1}$)
K	Thermal conductivity ($\text{W m}^{-1} \text{ }^\circ\text{C}^{-1}$)
K_i	Thermal conductivity of ice ($\text{W m}^{-1} \text{ }^\circ\text{C}^{-1}$)
K_s	Thermal conductivity of snow ($\text{W m}^{-1} \text{ }^\circ\text{C}^{-1}$)
k	Shortwave radiation extinction coefficient (m^{-1})
Q	Heat flux (W m^{-2})
Q_i	Flux in the ice layer (W m^{-2})
Q_h	Sensible heat flux to the air (W m^{-2})
Q_{le}	Latent heat flux to the air (W m^{-2})
Q_{rl}	Downward atmospheric longwave radiation (W m^{-2})

Q_{rnl}	Net longwave radiation ($W\ m^{-2}$)
Q_s	Sensible heat flux in snow layer ($W\ m^{-2}$)
Q_{sw}	Incident shortwave radiation ($W\ m^{-2}$)
Q_{swc}	Potential incident shortwave radiation with no cloud cover ($W\ m^{-2}$)
Q_t	Total net flux leaving the ice surface ($W\ m^{-2}$)
Q_w	Turbulent flux from river water to bottom of the ice sheet ($W\ m^{-2}$)
Q_z	Flux of shortwave radiation received at depth z in snow/ice layer
q_a	Specific humidity in the air ($kg\ kg^{-1}$)
q_s	Specific humidity at the surface ($kg\ kg^{-1}$)
R	Hydraulic radius (m)
T	Temperature ($^{\circ}C$)
T_a	Air temperature ($^{\circ}C$)
T_s	Surface temperature ($^{\circ}C$)
T_m	Temperature at ice/water interface ($^{\circ}C$)
T_w	Water temperature ($^{\circ}C$)
t	Time (s)
U	Wind speed ($m\ s^{-1}$)
U_w	Water speed ($m\ s^{-1}$)
VK	von Karman constant
Z	Depth below the surface (m)
Z_a	Height of meteorological observations (m)
Z_i	Ice thickness (m)
Z_n	Distance between computation nodes (m)
Z_o	Aerodynamic roughness length (m)
Z_r	Depth of penetration by shortwave radiation (m)

Z_s	Snow layer thickness (m)
Z_w	Depth of water (m)
α	Thermal diffusivity ($m^2 s^{-1}$)
ϵ	Longwave emissivity
λ	Latent heat of fusion ($J Kg^{-1}$)
ρ	Density ($kg m^{-3}$)
σ	Stefan-Boltzman constant ($W m^{-2} K^{-4}$)
τ	Momentum flux per unit area ($kg m^{-1} s^{-2}$)
ψ	Correction factor for atmospheric stability

Appendix **B.** SURFACE ENERGY BALANCE MODEL

```

PROGRAM Q(INPUT,OUTPUT,TAPES,TAPE6=OUTPUT,TAPES)
C  QGRIV3  REVISED AUGUST 1980
C  GORDON GREENE  GLERL, NOAA
REAL LE
COMMON IDAY, Z
DIMENSION T(500),Z(500)
5  FORMAT(2I4,5F6.0,F6.2)
7  FORMAT(2I4,8F10.1)
8  FORMAT(10X,20F5.1)
9  FORMAT(18)
DT=24 *3 6E3
DZ=2
LSNOW=20
LICE=20
LBOT=22
LFIX=LBOT+4
MELT=0
ABLA=0
ZSNOW=0
C INITIAL CONDITIONS ON JAN 10, 1976
C 4 CM OF ICE COVER. NO SNOW, TSURF=TAIR,TW=0 35
ZICE4 =
TW=0 35
TAIR=-19
SNOW=2 5
SNOFL=SNOW/(2 *30 )
Z(1)=0
LL=LFIX+80
DO 10 L=2,LL
10 Z(L)=Z(L-1)+DZ
DO 20 L=1,LL
20 T(L)=TW
T(LSNOW)=TAIR/2
T(LSNOW+1)=TAIR/4
T(LSNOW+2)=0
C READ IN FORCING DAILY METEOROLOGICAL DATA
DC 75 J-1,1000
READ(5,5) IYR, IDAY, U, TA, TD, P, SUN, TW
IF(EOF(5)) 90,15
15 IF(U EQ 0 ) U=1
U=IXAA,7
IF(IDAY C T 65) SNOFL=0
T(LFIX)=TW
C FIND EQUILIBRIUM SURFACE TEMPERATURE
CALL SEARCH(SUN,P,TA,U,Z,DZ,RN,S,H,LE,
1SNOFL,LICE,LSNOW,LBOT,ZSNOW,TD,T,TS,LFIX,
2ZICE,MELT,ABLA)
T(LSNOW)=TS
IF(IDAY EQ 10) T(LSNOW)=TA/2
C RECALCULATE THERMAL PROFILE
??
CALL TEVOL(T,Z,LSNOW,LICE,LFIX,DT,TW)
TOPICE=Z(LICE)
BOTICE=Z(LICE)
DO 30 L=LSNOW,LFIX
30 IF(T(L) LE 0 ) BOTICE=Z(L)
ZICE=BOTICE-TOPICE
LBOT=BOTICE/DZ+1
LFIX=LBOT+4
WRITE(6,7) IYR, IDAY, ZSNOW, ZICE, TA, TS, RN, S, H, LE
WRITE(6,8) (T(I), I=LSNOW, LFIX)
WRITE(8,7) IYR, IDAY, ZSNOW, ZICE, TA, TS, RN, S, H, LE
WRITE(8,8) (T(I), I=LSNOW, LFIX)
ICLK=LFIX-LSNOW
IF(ICLK LT 20) WRITE(8,9) ICLK
75 CONTINUE
90 CONTINUE
STOP
END
C
C
FUNCTION BB(TK)
BB=8.14E-11*(TK**4 )
RETURN
END
C
C

```

```

C FUNCTION HCOND(XW,XI,XA)
C ** ESTIMATE THERMAL CONDUCTIVITY **
  DIMENSION HK(3),X(3),XK(3)
  DATA HK/1.37E-3,4.2E-3,0.06E-3/
  X(1)=XW
  X(2)=XI
  X(3)=XA
  XKD=.0
  DO 2 I=1,3
    XK(I)=X(I)/HK(I)
    XKD=XKD+XK(I)
  2 CONTINUE
  DO 3 I=1,3
    XK(I)=XK(I)/XKD
  3 CONTINUE
  XLN=.0
  XLD=.0
  DO 4 I=1,3
    XLN=XLN+XK(I)*HK(I)*X(I)
    XLD=XLD+XK(I)*X(I)
  4 CONTINUE
  HCOND=XLN/XLD
  RETURN
END
??

C
C
C SUBROUTINE LONGRAD(ALB,P,TDK,IDAY,TAK,RH,QS,RLN,TS)
C PROGRAM TO COMPUTE NET LONGWAVE RADIATION BASED ON ANDERSON AND
C -RAY,FP 1967
C COMPUTATION OF PRECIP. WATER (MM) FROM BOLSENGA, 1967
  DIMENSION SUNB(24)
  XLAT=44.7
  D=IDAY
  TSK=TS+273.16
  TD=TDK+273.16
  TDF=(9./5.*TD)+32
  PL=-1.015+(0.035*TDF)
  PUAT=EXP(PL)*10
  DUST=10
  DEC=SIN(((D-173.)*360./365.+90.)/57.3)*23.45
  RU=SIN(((D-186.)*360./365.+90.)/57.3)*0.01671+1
  DO 80 I=1,24
    HR=FLOAT(I-1)
    CALL SPNTH(XLN,TD,DFC,WRN,.0,ALTD,AZMD,ANGI)
    CALL SOL(ANGI,ALTD,RU,DUST,PUAT,P,ALB,SUN,BEAM,HEM,EXT)
    SUNB(I)=SUN
  80 CONTINUE
  B=24.*60
  CALL TRAP(0.,B,24,SUNB,XINT)
  QSC=XINT
  R=.33
  ES=UAPORA(TAK)
  EA=RH*ES
  X1=BB(TAK)*24.*60
  X2=(SQRT(ES)-SQRT(EA))
  X3=(QS/QSC)**2
  RSKY=X1-(228.+11.16*X2-A)*X3
  RS=BB(TSK)*24.*60
  RLN=RSKY-RS
  RETURN
END

C
C
C SUBROUTINE RADZ(LSNOW,LBOT,Z,RSN,T,LICE)
C DERIVED FROM MAYKUT AND UNTERSTEINER, JGR, UO L 76 P1550
  DIMENSION T(500), Z(500)
  LICE1=LICE+1
  DO 10 L=LICE1,LBOT
    ZL=ABS(Z(LSNOW)-Z(L))
    C=.44
    XK=.02
    TRAD=RSN*(XK/C)*EXP(-XK*ZL)
    T(L)=T(L)+TRAD
  10 CONTINUE
??

```

RETURN
END

CC

```
SUBROUTINE SEARCH(SUN,P,TA,U,Z,DZ,RN,S,H,LE,SNOFL,LICE,LSNOW
1 LBOT,ZSNOW,TD,T,TS,LFIX,ZICE,MELT,ABLA)
DIMENSION T(500),BAL(80),G(80)
DIMENSION Z(500)
REAL LE
TK=273.16
TAK=TA+TK
TDK=TD+TK
XLVD=6.E4*1.4.4
ZSNOW=ZSNOW+SNOFL-ABLA
IF(ZSNOW.LT.0)ZSNOW=0
IF(ZICE.LT.0)ZSNOW=0
LOUSE=ZSNOW/DZ
LSNOW=LICE-LOUSE
T(LSNOW)=-1
IF(TA.LT.0)T(LSNOW)=TA
G(1)=40
G(2)=-60
FLAG=10
CALL SLFLUX(TAK,G(1),T,DZ,LSNOW,LICE,P,TDK,U,BAL(1),RN,SUN,S,H,LE
1,ZICE,ZSNOW,FLAG,LBOT)
FLAG=-10
CALL SLFLUX(TAK,G(2),T,DZ,LSNOW,LICE,P,TDK,U,BAL(2),RN,SUN,S,H,LE
1,ZICE,ZSNOW,FLAG,LBOT)
DO 37 K=3,80
CALL SECANT(K,BAL,G,GUNOW)
G(K)=GUNOW
TS=GUNOW
CALL SLFLUX(TAK,G(K),T,DZ,LSNOW,LICE,P,TDK,U,BAL(K),RN,SUN,S,H,LE
1,ZICE,ZSNOW,FLAG,LBOT)
TEST=ABS(BAL(K))
IF(TEST.LT.1)GO TO 38
37 CONTINUE
38 CONTINUE
PRINT*, 'NUMBER OF ATTEMPTS ON TS',K
IF(ZSNOW.GT.0.AND.TS.GE.0)GO TO 80
IF(TS.GE.0)TS=0
ABLA=0
GO TO 90
80 TS=0
CALL SLFLUX(TAK,0,T,DZ,LSNOW,LICE,P,TDK,U,ARF,RN,SUN,S,H,
1LE,ZICE,ZSNOW,FLAG,LBOT)
CALL SNOFLT(T,LICE,TAK,MELT,H,LE,RN,LSNOW,DZ,ABLA)
90 RETURN
END
```

C
??

C

```
SUBROUTINE SECANT(KOUNT,BAL,TGUS,GUNOW)
DIMENSION BAL(80),TGUS(80)
K=KOUNT
F1=BAL(K-2)
F2=BAL(K-1)
T1=TGUS(K-2)
T2=TGUS(K-1)
GUNOW=T2-(((T2-T1)*F2)/(F2-F1))
RETURN
END
```

C
C

```
      SUBROUTINE SLFLUX(TAK,TS,T,DZ,LSNOW,LICE,P,TDK,U,BAL,RN,SUN,S,  
1H,LE,ZICE,ZSNOW,FLAG,LBOT)  
      DIMENSION Z(500)  
      COMMON IDAY,Z  
      REAL LE,LHEAT  
      DIMENSION T(500)  
      XLYD=.6E4*1.44  
      TK=.273.16  
      TSK=TS+TK  
      IF(FLAG.LT.0)GO TO 70  
      ALB=.55  
      IF(ZSNOW.C.T.0)ALB=.85  
      IF(TAK.C.T.TK)ALB=.40  
      RSN=SUN*(1.-ALB)  
      IF(ZSNOW.C.T.0)GO TO 70  
      IF(ZICE.LE.0)GO TO 70  
      CALL RADZ(LSNOW,LBOT,Z,RSN,T,LICE)  
      RSN=0  
70  CONTINUE  
      RH=VAPORA(TDK)/VAPORA(TAK)  
      CALL LONGRAD(ALB,P,TDK,IDAY,TAK,RH,SUN,RLN,TS)  
      RN=RSN+RLN  
      CON.4 2E-3  
      IF(LSNOW.LT.LICE.AND.(LSNOW.LT.0).CON.6 4E-4  
      S=(CON/DZ)*(T(LSNOW+1)-TS)*XLYD  
      AIRDEN=.34838*(P/TAK)*1.E-3  
      ZA=1000.  
      ZO=0.07  
      E2=VAPORA(TAK)  
      E1=VAPORI(TSK)  
      Q=(.622*E2*RH)/(P-.378*E2)  
      QG=(.622*E1*1.)/(P-.378*E1)  
      LHEAT=.670  
      IF(TSK.GE.TK)LHEAT=.590  
      CALL TURB(TAK,TSK,ZA,ZO,Q,QG,U,AIRDEN,LHEAT,H,LE)  
      BAL=RN+S+H+LE  
      RETURN
```

??

END

C
C

```
      SUBROUTINE SNOMLT(T,LICE,TAKMELT,XHZ,XLEZ,RLN,LSNOW,DZ,ABLA)  
      DIMENSION T(500)  
      HFUS=.80  
      SNODEN=.35  
      SNOCAP=.48*SNODEN  
      CM=HFUS*SNODEN  
      XLH=.590  
      XLHF=.670  
      TK=.273.16  
      T(LICE)=0  
      T(LICE-1)=0  
      S=0  
      IF(MELT.EQ.1)RMDR=0  
      FLUXIN=RLN+XHZ+XLEZ+RMDR  
      RMDR=0  
      LFST=LSNOW+1  
      LLST=LICE-1  
      ABLR=0  
      IF(MELT.EQ.1)ABLA=FLUXIN/CM  
      IF(MELT.EQ.1)GO TO 21  
      DO 20 L=LFST,LLST  
      HCOUNT=(0.-T(L))*DZ*SNOCAP  
      IF(HCOUNT.EQ.0)GO TO 20  
      IF(FLUXIN.GE.HCOUNT)T(L)=0  
      IF(T(L).LT.0)MELT=0  
      IF(T(L).GE.0)MELT=1  
      IF(FLUXIN.GE.HCOUNT)FLUXIN=FLUXIN-HCOUNT  
      IF(FLUXIN.LT.HCOUNT)RMDR=FLUXIN  
      IF(FLUXIN.LT.HCOUNT)FLUXIN=0  
      IF(FLUXIN.LT.HCOUNT)GO TO 21  
20  CONTINUE  
21  CONTINUE  
      IF(MELT.EQ.1)T(LICE)=T(LICE-1)  
      RETURN  
      END
```

C
C

```
SUBROUTINE SOL(ANGI,ALTD,RV,DUST,PWAT,P,ALB,SUN,BEAM,HEM,  
1EXT)  
  ANGRAD( DEG )=DEG/57.29557  
  OKER(AL,ALTD)=1./((SIN(AL)+.15*((ALTD+3.885)**(-1.253)))  
  AI=ANGRAD(ANGI)  
  AL=ANGRAD(ALTD)  
  EXT=(2./RV**2)*SIN(AL)  
  IF(EXT.LE.0) EXT=0.  
  XM=OKER(AL,ALTD)*(P/1013.  
  ABSD=-0.089*((P*XM)/1013.))**0.75,  
??
```

```
  I=0.174*((PWAT*XM)/20)**0.6  
  SCAT=-0.083*((DUST*XM)**0.9)  
  BEAM=(2./RV**2)*SIN(AI)*EXP(ABSD+SCAT)  
  IF(BEAM.LE.0) BEAM=0.  
  RSCAT=0.5*EXT*(1-EXP(SCAT))  
  DIFF=RSCAT  
  SOLAR=BEAM+DIFF  
  BACSKT=0.5*SOLAR*ALB*(1-EXP(SCAT))  
  HEM=DIFF+BACSKT  
  SUN=BEAM+HEM  
  RETURN  
  END
```

C
C

```
SUBROUTINE SPATH(XLAT,DEC,HR,SLOPE,EXPO,ALTD,AZMD,ANGI)  
  ANGRAD( DEG )=DEG/57.29557  
  ANGDEG( RAD )=RAD*57.29557  
  H=ANGRAD((HR/24)*360.-180.)  
  X=ANGRAD(XLAT)  
  D=ANGRAD(DEC)  
  E=ANGRAD(EXPO-180.)  
  S=ANGRAD(SLOPE)  
  COSZ=(SIN(X)*SIN(D)+COS(X)*COS(D))*COS(H)  
  Z=ACOS(COSZ)  
  ZD=ANGDEG(Z)  
  SINA=(COS(D)*SIN(H))/SIN(Z)  
  COSA=(SIN(X)*COS(Z)-SIN(D))/(COS(X)*SIN(Z))  
  A=ATAN2(SINA,COSA)  
  COSI=(COS(S)*COS(Z)+SIN(S)*SIN(Z))*COS(A-E)  
  XI=ACOS(COSI)  
  AL=ANGRAD(90.-ZD)  
  ALTD=ANGDEG(AL)  
  AZMD=ANGDEG(A)  
  ANGI=ANGDEG(ANGRAD(90.)-XI)  
  IF (ALTD.LE.0) ALTD=0  
  IF (ANGI.LE.0) ANGI=0  
  IF (ALTD.EQ.0) ANGI=0  
  RETURN  
  END
```

C
C

```
SUBROUTINE TEVOL(T,Z,LSNOW,LICE,LZ,DT,TW)  
  DIMENSION T(500),Z(500)  
  DIMENSION A(500),B(500),C(500),D(500)  
  C1=2  
  A(LSNOW)=1  
  B(LSNOW)=1  
  C(LSNOW)=1  
  D(LSNOW)=T(LSNOW)  
  A(LZ)=1  
??
```

```

      B(LZ)=1
      C(LZ)=1
      D(LZ)=T(LZ)
      LZM1=LZ-1
      LSNOW1=LSNOW+1
      DO 80 L=LSNOW1, LZM1
      ZU2=(ABS(Z(L)-Z(L-1)))**2
      ZB2=(ABS(Z(L)-Z(L+1)))**2
      IF(L.LT.LICE) DIF=39.E-4
      IF(L.LT.LICE) GO TO 50
      IF(T(L).GE.0.0) DIF=0.1
      IF(T(L).GE.0.0) GO TO 50
      XA=0.05
      XU=(1.-XA)*EXP(C1*T(L))
      XI=1.-XU-XA
      DXDT=C1*XU
      CON=HCOND(XU,XI,XA)
      CAP=XU+0.5*XI+80.*DXDT
      DIF=CON/CAP
50  CONTINUE
      FU=(DIF*DT)/ZU2
      FB=(DIF*DT)/ZB2
      A(L)=-FU
      B(L)=1.+FU+FB
      C(L)=-FB
      D(L)=T(L)
80  CONTINUE
      CALL TRIMP(LSNOW,LZ,A,B,C,D,T)
90  CONTINUE
      RETURN
      END

C
C
      SUBROUTINE TRAP(A,B,N,SUNB,XINT)
C  PROGRAM FOR NUMERICAL INTEGRATION USING THE TRAPEZOIDAL RULE
C  FROM BECKETT AND HURT. 1967
      DIMENSION SUNB(24)
      H=(B-A)/N
      XINT=0
      X=A+H
      NM=N-1
      DO 50 I=1,NM
      FX=SUNB(I)
      XINT=XINT+2.*FX
      X=X+H
50  CONTINUE
      FX=SUNB(N)
      XINT=(XINT+FX)*H/2
      RETURN
      END

??

C
C
      SUBROUTINE TRIMP(NF,NL,A,B,C,D,T)
      DIMENSION A(500),B(500),C(500),D(500)
      DIMENSION BETA(500),GAMMA(500),T(500)
      N1=NF+1
      N2=NF+2
      M1=NL-1
      M=NL-2
      GAMMA(NF)=T(NF)
      BETA(NF)=0.0
      GAMMA(N1)=(D(N1)-A(N1)*T(NF))/B(N1)
      BETA(N1)=C(N1)/B(N1)
      DO 1 L=N2,M1
      DENOM=B(L)-A(L)*BETA(L-1)
      GAMMA(L)=(D(L)-A(L)*GAMMA(L-1))/DENOM
1  BETA(L)=C(L)/DENOM
      DO 2 K=1,M
      L=NL-K
2  T(L)=GAMMA(L)-BETA(L)*T(L+1)
      RETURN
      END

```

```

C
C
SUBROUTINE TURB(TAK, TS, ZA, ZO, Q, QG, U, AIRDEN, XLH, H, XLE)
G=981
F=6 E4*1 4 4
TGM=SQRT(TAK*TS)
UK=0 41
C INITIAL GUESS FOR USTAR
C=24*AIRDEN
USTAR=(UK*U)/(ALOG(ZA/ZO))
C INITIAL GUESS FOR L
S=U*U*TGM/(G*(TAK-TS))
XL=S/ALOG(ZA/ZO)
DO 80 I=1,10
IF(XL) 5,5,7
C UNSTABLE
5 X=(1.-16 *ZA/XL)** 25
SY2=2 *ALOG((1 +X**1/2 )
SY1=2 *ALOG((1 +X)/2)+ALOG((1 +X**X)/2 1 - 2 *ATAN(X))+1 570796
GO TO 9
C STABLE
7 SY1=-5 2*ZA/XL
C STRONGLY STABLE
IF(ZA/XL GT.1.) SY1=-5 2*(1 +ALOG(ZA/XL))
SY2=SY1
C COMPUTE USTAR, TSTAR, XL
9 USTAR=U*UK/(ALOG(ZA/ZO)-SY1)
XL=S*(ALOG(ZA/ZO)-SY2)/(ALOG(ZA/ZO)-SY1)**2
??

22 CONTINUE
CH=UK*USTAR/(U*(ALOG(ZA/ZO)-SY2))
H=C*U*CH*(TAK-TS)*F
XLE=AIRDEN*XL*CH*U*(Q-QG)*F
RETURN
END

C
C
FUNCTION VAPORA(TK)
C LOWE, P., J A M., VOL16 1977
A0=6984 505294
A1=-188.9039310
A2=2 133357675
A3=-1 288580973E-2
A4=4 393587233E-5
A5=-8 023923082E-8
A6=6 136820929E-11
SATW=A0+TK*(A1+TK*(A2+TK* TK*(
1A4+TK*(A5+A6*TK))))))
VAPORA=SATW
RETURN
END

```

```

C
C
FUNCTION VAPORI(TK)
c LOUE.P. J A M U O L 16 1977
TC=TK-273.16
B0=6.189177956
B1=5.03469897E-1
B2=1.886013408E-2
B3=4.176223716E-4
B4=5.824720280E-6
B5=4.838803174E-8
B6=1.838826904E-10
SATI=B0+TC*(B1+TC*(B2+TC*(B3+TC*(
1B4+TC*(B5+B6*TC))))))
A0=6984.585294
A1=-188.9039310
A2=2.133357675
A3=-1.288580973E-2
A4=4.393587233E-5
A5=-8.023923082E-8
A6=6.136820929E-11
SATU=A0+TK*(A1+TK*(A2+TK*(A3+TK*(
1A4+TK*(A5+A6*TK))))))
IF(TK.LT.273.16)00 TO 10
VAPORI=SATU
GO TO 20
10 CONTINUE
VAPORI=SATI
20 CONTINUE
RETURN
END
/EOF
??
ND OF FILE

```

Appendix C. ANALYTIC ICE GROWTH MODEL

```

PROGRAM DEGD(INPUT,OUTPUT,TAPES,TAPES-OUTPUT,TAPE?)
C PROGRAM TO COMPUTE ICE THICKNESS FOR 1976 ST. LAURENCE
C BASED ON ASHTON, 1978 AND MICHEL, 1971
50 FORMAT(2I4,2F6.0,10X,F6.2)
60 FORMAT(2I4,5F10.1)
ALPH=0.5
FAC=3.49
DT=1.44E3
DEN=0.92
XLH=80.0
H2=0
H3=0
HTOT2=0
HTOT3=0
DD1=0
SNOW=0
5NOFL=.8/(2.*30.)
DO I=1,225
READ(5,50) IYR, IDAY, U, TA, TU
IF(IYR.EQ.75) GO TO 100
C TURBULENT EXCHANGE COEF BASED ON WILLIAMS(1963)
C UNITS OF XHA ARE CALCM-2MIN-1C-I
XHA=24./DT
DELT=0.-TA
IF(IYR.EQ.75.OR.IDAY.LT.10) GO TO 90
IF(IDAY.GT.100) GO TO 90
DD1=DD1+DELT
C ASSUME THAT TA NOT EQUALS AND SNOW PRESENT
A=H2/((5.2E-3)*60.
8.1/XHA
SNOW=SNOW+SNOFL
IF(IDAY.GT.80) SNOW=0
C=SNOW/((6.4E-4)*60.)
H2=(DELT*DT)/((A+B+C)*DEN*XLH)
HTOT2=HTOT2+H2
C ASSUME TA=TS AND SNOW PRESENT
D=(HTOT3+(5.2E-3/6.4E-4)*SNOW)**2
E=(2.*5.2E-3/(DEN*XLH))*DELT*3600 t 2 4
F=HTOT3+(5.2E-3/6.4E-4)*SNOW
H3=SQRT(D+E)-F
HTOT3=HTOT3+H3
C ASSUME THAT TA=TS AND NO SNOW
HTOT1=FAC*SQRT(DD1)
90 CONTINUE
WRITE(6,60) IYR, IDAY, TA, DD1, HTOT1, HTOT2, HTOT3
WRITE(7,60) IYR, IDAY, TA, DD1, HTOT1, HTOT2, HTOT3
100 CONTINUE
STOP
END
??

```

Appendix D. ANALYTIC ICE DECAY MODEL

```

PROGRAM MELT(INPUT,OUTPUT,TAPES,TAPE6-OUTPUT)
C PROGRAM TO COMPUTE ICE MELT FROM ASHTON, 1973
C STARTING WITH OBSERVED MAX OF 66 CM ON 69 1976
C ASHTON'S QU IN W M-2 UNITS IN JOULES,METERS,KG,SEC
REAL N,NI
50 FORMAT(5X,I3,6X,F6.0,18X,F6.2)
60 FORMAT(2I5,3F8.2)
U=0.5
D=20.0
DEN=0.92E3
FUS=3.34E5
CON=2.2
TM=0
DT=8.64E4
NI=0.66
DOLEE I=1.100
READ(5,50) IDAY,TA,TW
IF(IDAY LT 69 OR IDAY GT 100) GO TO 100
IF(TA E 0) TA=-0.01
TS=TA
QU=1187 *TW*(U**0.8)/(D**0.2)
DO 90 J=1,500
N=NI-(J*0.0004)
T1=(-1 *DEN)*FUS*(N-NI)/QU
T2=CON *DEN *FUS*(TM-TS)/(QU**2)
T3=1 -(QU*N)/(CON*(TM-TS))
T4=1 -(QU*NI)/(CON*(TM-TS))
TS=T3/T4
IF(TS LE 0) GO TO 90
RS=T1-T2 *ALOG(T5)
BAL=ABS(DT-RS)
IF(BAL LE 3000) GO TO 91
90 CONTINUE
91 NT=N
N=N*100
WRITE(6,60) IDAY,J,TA,TW,N
100 CONTINUE
STOP
END
/EOR
??

```

Appendix E. METEOROLOGICAL INPUT DATA, OGDENSBURG, N.Y.

